Draft version November 30, 2011
Preprint typeset using LaTeX style emulateapj v. 14/09/00

HIGH-RESOLUTION ROTATION CURVES OF LSB GALAXIES: MASS MODELS

W.J.G. de Blok[1]
Australia Telescope National Facility
PO Box 76, Epping NSW 1710, Australia
edeblok@atnf.csiro.au

Stacy S. McGaugh
Department of Astronomy, University of Maryland
College Park, MD 20742-2421, USA
ssm@astro.umd.edu

AND

Vera C. Rubin
Department of Terrestrial Magnetism
Carnegie Institution of Washington
5241 Broad Branch Rd., N. W.
Washington, D. C. 20015, USA
rubin@dtm.ciw.edu
Draft version November 30, 2011

ABSTRACT

We present mass models for a sample of 30 high-resolution rotation curves of low surface brightness (LSB) galaxies. We fit both pseudo-isothermal (core-dominated) and Cold Dark Matter (CDM) (cusp-dominated) halos for a wide variety of assumptions about the stellar mass-to-light ratio. We find that the pseudo-isothermal model provides superior fits. CDM fits show systematic deviations from the data, and often have a small statistical likelihood of being the appropriate model. The distribution of concentration parameters is too broad, and has too low a mean, to be explained by ΛCDM. This failing becomes more severe as increasing allowance is made for stellar mass: NFW fits require uncomfortably low mass-to-light ratios. In contrast, the maximum disk procedure does often succeed in predicting the inner shape of the rotation curves, but requires uncomfortably large stellar mass-to- light ratios. The data do admit reasonable stellar population mass-to-light ratios if halos have cores rather than cusps.

Subject headings: galaxies: kinematics and dynamics — galaxies: fundamental parameters — dark matter

1. INTRODUCTION

1.1. *LSB Galaxies*

Over the last five years the rotation curves of Low Surface Brightness (LSB) galaxies and the constraints they impose on cosmological theories have received much attention in the literature. An LSB galaxy is usually defined as a disk galaxy with an extrapolated central disk surface brightness $\gtrsim 1$ mag arcsec^{-2} fainter than the typical value for "normal" High Surface Brightness (HSB) spiral galaxies (Freeman 1970). Colors, metallicities, gas-fractions, and extensive population synthesis modelling all support the idea that LSB galaxies are unevolved galaxies with low (current and past) star formation rates (e.g. van der Hulst et al. 1993; McGaugh & Bothun 1994; McGaugh 1994; McGaugh & de Blok 1997; de Blok, van der Hulst & Bothun 1995; van den Hoek et al. 2000; Bell et al. 2000). See Bothun, Impey & McGaugh (1997) for a review.

The observation that LSB and HSB galaxies follow the same Tully-Fisher (TF) relation requires (in the conventional picture) that LSB galaxies are dominated by dark matter (DM) (Zwaan et al. 1995; Sprayberry et al. 1995; Verheijen 1997; de Blok & McGaugh 1996). For reasonable stellar mass-to-light ratios $\Upsilon_\star$ low surface brightness implies low stellar density. Yet, the extended, low surface density stellar disks cannot be the major contributors to the dynamics in LSB galaxies, as no shift in the zero-point of the TF relation with surface brightness is observed. This contrasts with the dominance of the stellar population in HSB galaxies of similar luminosity.

The modest $\Upsilon_\star$ values as implied by the blue colors and the (baryonic) TF relation, together with the diffuseness of the stellar disks make analyses of the DM distribution in LSB galaxies less ambiguous than in HSB galaxies where the stellar component can be significant even for fairly low $\Upsilon_\star$ values. LSB galaxies are therefore ideal laboratories for measuring the distribution of dark matter for comparison with predictions of theories of galaxy formation.

For example, one of the results of numerical Cold Dark Matter (CDM) simulations is a so-called "universal halo mass density profile" (Navarro, Frenk & White 1996), commonly known as a "NFW profile." NFW (and all CDM) mass density profiles are characterized by steep central cusps. This is in contrast with the other commonly used "classic" pseudo-isothermal sphere halo model which is characterized by a constant density core. The parame-

[1] Bolton Fellow

ters of the NFW mass density distribution are related to the mass of the halo and the density of the universe at the time of collapse and are therefore set by the cosmology. As these parameters can be determined from observations, this opens the possibility of testing the NFW CDM model as well its underlying assumptions.

A first analysis of LSB galaxy HI rotation curves by de Blok & McGaugh (1997) indicated that they did not rise as steeply as their HSB counterparts of similar luminosity, contrary to CDM predictions. The mass distribution in LSB galaxies is more extended and of lower density than in HSB galaxies (de Blok & McGaugh 1996).

Other results also indicate that the steep rotation curves implied by CDM are hard to reconcile with the observed shallow rotation curves of dwarf galaxies (Moore 1994; Flores & Primack 1994; Blais-Ouellette, Amram & Carignan 2001; Côté, Carignan & Freeman 2000). To explain this discrepancy the possibility of redistribution of the (cuspy) DM due to violent star-formation (thus creating the observed cores) was sometimes raised, but this has been shown to be inconsistent with other observational data (Mac Low & Ferrara 1998).

McGaugh & de Blok (1998) argued that the shapes of rotation curves of LSB galaxies were inconsistent with those predicted by the NFW prescription. This could not be explained by the effects of star formation as the larger masses of LSB galaxies would require large bursts in order to redistribute matter on large scales. Their quiescent evolutionary history argues strongly against this (van den Hoek et al. 2000).

This comparison with the CDM model is often dismissed because of the limited resolution of the observed HI curves. The early HI LSB rotation curves were obtained using the VLA and WSRT radio synthesis telescopes. The relatively large beams of these instruments resulted in rotation curves with only a limited resolution. de Blok & McGaugh (1997) did however show that for the best resolved cases the effects of beam smearing were not strong enough to explain the observed shallow curve as simply the result of a steep NFW model curve affected by beam-smearing. Similar results were found for more fashionable cosmologies, such as ΛCDM ($\Omega_m \sim 0.3,\ \Omega_\Lambda \sim 0.7$), though with smaller discrepancies.

Even so, the theoretical debate now seems to have settled on halos with cusps even steeper than NFW halos (Moore et al. 1999), thus worsening the possible conflict between the data and the simulations. From the observational point of view the easiest and least ambigous way to test the reality of these discrepancies is to measure high-resolution rotation curves.

1.2. *Optical rotation curves*

Optical Hα rotation curves of five LSB galaxies from the sample of de Blok, McGaugh & van der Hulst (1996) (BMH) were presented in Swaters, Madore & Trewhella (2000) (SMT). Though SMT found that for two of the five galaxies the inner slopes of the rotation curves were steeper than derived from the HI observations, this difference does not affect the BMH conclusion that LSB rotation curves have shallower slopes than HSB rotation curves of similar amplitude. Because of these steeper slopes, SMT derive higher maximum-disk $\Upsilon_\star$ values (in some cases > 10), strengthening one of the conclusions from de Blok & McGaugh (1997) that the maximum $\Upsilon_\star$ values in LSB galaxies are too large to be accommodated by reasonable star formation histories and Initial Mass Functions. Such high values are inconsistent with the existence of a baryonic TF-relation (McGaugh et al. 2000).

A different approach was taken by van den Bosch et al. (2000). They attempted to apply a rigorous correction for beamsmearing to the BMH HI data, and thus to derive the true "infinite resolution" rotation curve. They conclude that the data are not of high enough resolution to accept or reject the NFW hypothesis with any significance. However, as they use a modified NFW profile with the inner slope of the mass-density distribution as an (additional) free parameter, it is not clear how significant this conclusion is. The usual 3-parameter rotation curve fits are already under-constrained; adding another parameter does not improve the significance of the results. Furthermore, in some cases they find such low values for the inner slope that their NFW-halos effectively become core-dominated. These halos do of course fit the data, but do not occur in CDM simulations.

The general picture as derived from early observations of rotation curves of LSB galaxies therefore still holds: LSB galaxies are unevolved, low density galaxies, dominated by DM. Their rotation curves have shallower slopes than those of HSB galaxies of similar amplitude, and the shape of the best-resolved LSB curves are not necessarily consistent with the NFW rotation curve shapes.

1.3. *New data*

In this paper we present an analysis of high-resolution high-quality hybrid Hα/HI rotation curves of a sample of 30 LSB galaxies. Of this sample 26 curves were taken from the large sample of 50 LSB galaxies presented in McGaugh, Rubin & de Blok (2001) (herafter Paper I). In that paper an extensive description is given of the data, the sample and reduction method. We also refer to that paper for a comparison of the new Hα data with the BMH HI curves. We also re-analyse the data for an additional 5 curves taken from Swaters, Madore & Trewhella (2000). In this paper we derive mass models under various assumptions for $\Upsilon_\star$ and fit these models both with NFW halos and pseudo-isothermal halos. A similar analysis for a different set of rotation curves of dwarf and LSB galaxies is given in de Blok & Bosma (2001).

In Section 2 we discuss the sample, and discuss the derivation of the rotation curves. We also show internal and external comparisons of the data and discuss possible systematics. In Section 3 we discuss the various mass models. Section 4 contains the results of the model fitting. Section 5 discusses the implications for the various halo models. In Section 6 we turn our attention to the maximum disk and a summary is given in Section 7.

When using absolute distances we have used a Hubble constant $H_0 = 75$ km s^{-1} Mpc^{-1}.

2. THE DATA

2.1. *Sample and raw data*

The data and reduction methods have been extensively described in Paper I. In summary, we use long-slit major axis spectra taken with the 4-m telescope at Kitt Peak in

June 1999 and February 2000 and the 100″ telescope at Las Campanas in November 1998. Velocities were derived from the intensity weighted centroid of the Hα and [NII] lines.

As the aim of this excercise is to derive mass models which can yield significant constraints on the distribution of DM we select only the 26 high quality galaxies from Paper I. We split this high-quality sample in two sub-samples. Sample I contains LSB galaxies from BMH and van der Hulst et al. (1993) for which a full set of photometry and HI data is available. In Sample I we also include the five galaxies presented in SMT. For these galaxies HI and optical photometry are taken from BMH. Tables 1 and 2 contain a full list of the galaxies analysed here, along with some of their global parameters.

Sample II consists of ESO-LV and UGC LSB galaxies, for which an optical rotation curve is available but no optical or HI photometry.

For the galaxies in Sample I, HI observations are available which often extend to larger radii than the Hα data. To make the best use of both types of data, we have constructed hybrid rotation curves. These consist of the Hα data over the range of radii where available, and 21-cm data to define the outermost points. No attempt has been made to "average" the different types of data: Hα is given precedence over the range of radii where it is available.

2.2. *Derivation of the smooth curves*

One of the main assumptions made when deriving mass models from rotation curves is that the gas and stars trace circular orbits in an axisymmetric potential. Though the shape of the optical rotation curves in Paper I is well-defined, the scatter between individual datapoints means we cannot simply use the raw rotation curves to estimate the radial run of the gravitational potential. For this one needs a smooth curve which retains real small-scale details, but without the observational scatter.

The method most often used to produce these smooth curves is to fit splines to the data. Here we use have used a robust version of this procedure (local regression, see Loader 1999). The smooth curves were rebinned to a bin width of 2″. The error bars in the rebinned data points consist of two components: one due to observational errors caused by the measurement uncertainties in the individual raw datapoints (for this we use the average weighted measurement error in each bin), and an additional component caused by differences between approaching and receding sides and non-circular motions (which we define as the difference between the weighted mean raw velocity and the velocity implied by the spline fit at that radius). For the final error estimate these two uncertainties were added quadratically.

For some high S/N data points the error bars become unrealistically small (sometimes less than 1 km s^{-1}). This has no physical significance and simply tells us that the profile centroids were well-determined. These small error bars can however easily dominate any model fit and can severely bias χ^2 values or goodness-of-fit parameters. For this reason, and as the observational and physical uncertainties (slit position, streaming motions) make it difficult to determine a physically meaningful rotation velocity with an accuracy of more than a few km s^{-1}, we have imposed a minimum error on each point of 4 km s^{-1} (before inclination correction). The curves were corrected for inclination using the values given in Tables 1 and 2.

The end result is a smooth representation of the data, which is reproducible and as objective as possible, to use as input for the mass models. Figure 1 show overlays of both the raw hybrid curves and the smooth versions. It is easy to verify that no systematic differences in slope or shape have been introduced. The error bars in the smooth curves are also a good representation of the uncertainties in the underlying raw data.

Table 3 contains the hybrid smooth rotation curves. For each galaxy we list the radii in arcsec, as well as in kpc, together with the observed rotation velocities and the uncertainties in these values. Also included are the rotation curves for the gas component (already included is the factor 1.4 mass scaling for He), the disk component (values listed assume $\Upsilon_\star(R) = 1.0$), and where applicable the bulge component (also for $\Upsilon_\star(R) = 1.0$.

2.3. *Comparing the smooth curves*

As noted above, we have included the five LSB galaxies presented in SMT in our Sample I. As SMT show their raw data and derived smooth curves, we can compare both sets of smooth rotation curves to investigate possible systematics in our respective methods. This is done in Fig. 2. It is clear that the correspondence between both velocities and errorbars is good and the differences are minor. In most cases (F568-1, F568-V1 and F574-1) both sets agree at (better than) the 1σ level. Small remaining differences are usually caused by a slightly different estimate of the velocities in sparsely sampled parts (F563-V2 and F568-3). The SMT curve for F563-V2 (Fig. 2, top-left) is slightly higher than our curve in the inner parts, but falls below ours in the outer parts. The sparseness of optical data points in the outer parts and different interpretations of the continuity between HI and optical data are probably the main cause of this difference. For F568-3 (Fig. 2, bottom) we find a small ($\lesssim 1\sigma$) systematic difference between both smooth curves. This galaxy has been measured independently by SMT and by us (Paper I). These raw data sets agree in detail, and the difference must therefore be due to a slightly different interpretation of the sparse raw data. In summary, the smooth curves we present here give a good and reproducable representation of the data.

3. MASS MODELS

In order to find the signature of the dark halo one needs to model the observed rotation curve using a number of separate dynamical components, described below.

3.1. *Stellar component*

To model the stellar disk, the R-band photometry presented in de Blok, van der Hulst & Bothun (1995) was used. The rotation curve of the disk was computed following Casertano (1993) and Begeman (1987). The disk was assumed to have a vertical sech^2 distribution with a scale height $z_0 = h/6$ (van der Kruit & Searle 1981). The rotation curves of the stellar component were resampled at the same radii as the smooth curves. We assume $\Upsilon_\star$ is constant with radius. While one expects some modest

variation in $\Upsilon_\star$ with radius (de Jong 1996), the color gradients in LSB galaxies tend to be small, so this effect is not likely to be significant.

3.2. *Gas disk*

The HI surface density profiles presented in BMH and van der Hulst et al. (1993) were used. They were scaled by a factor of 1.4 to take the contribution of helium and metals into account. Their rotation curve was derived assuming the gas was distributed in a thin disk. The gas rotation curves were resampled at the radii of the smooth observed rotation curve.

3.3. *Dark halo*

The dark halo component differs from the previous two in that we are interested in parametrizing this component assuming some fiducial model. The choice of this model is the crux of most of the DM analyses in the literature, and many models exist. These can be broadly distinguished in two groups: halo models with a core, and halo models with a cusp. An example of the first category is the pseudo-isothermal halo, an example of the latter the CDM NFW halo.

As one of the goals of this paper is to assess the relevance of either category to the high-resolution LSB galaxy rotation curves, we will present models derived using both models. We do realize there are many intermediate models described in the literature that probably can fit our data equally well. However, our goal here is simply to see where the data lead us: is there a preference for models with a core or with a cusp? We now describe the details of both models.

3.3.1. *Pseudo-isothermal halo*

The spherical pseudo-isothermal halo has a density profile

$$\rho_{ISO}(R) = \rho_0 \Big[1 + \Big(\frac{R}{R_C}\Big)^2\Big]^{-1}, \quad (1)$$

where ρ_0 is the central density of the halo, and R_C the core radius of the halo. The corresponding rotation curve is given by

$$V(R) = \sqrt{4\pi G \rho_0 R_C^2 \Big[1 - \frac{R_C}{R}\arctan\Big(\frac{R}{R_C}\Big)\Big]}. \quad (2)$$

The asymptotic velocity of the halo, V_∞, is given by

$$V_\infty = \sqrt{4\pi G \rho_0 R_C^2}. \quad (3)$$

To characterize this halo only two of the three parameters (ρ_0, R_C, V_∞) are needed, as equation (3) determines the value of the third parameter.

3.3.2. *NFW halo*

The NFW mass density distribution takes the form

$$\rho_{NFW}(R) = \frac{\rho_i}{(R/R_s)\,(1 + R/R_s)^2} \quad (4)$$

where R_s is the characteristic radius of the halo and ρ_i is related to the density of the universe at the time of collapse. This mass distribution gives rise to a halo rotation curve

$$V(R) = V_{200}\left[\frac{\ln(1+cx) - cx/(1+cx)}{x[\ln(1+c) - c/(1+c)]}\right]^{1/2}, \quad (5)$$

where $x = R/R_{200}$. It is characterized by a concentration parameter $c = R_{200}/R_s$ and a radius R_{200}. These are directly related to R_s and ρ_i, but are used instead as they are a convenient way to parametrize the rotation curve. The radius R_{200} is the radius where the density contrast exceeds 200, roughly the virial radius (Navarro, Frenk & White 1996). The characteristic velocity V_{200} of the halo is defined in the same way as R_{200}. These parameters are not independent and are set by the cosmology.

3.4. *Mass-to-light ratios and weighting*

One of largest uncertainties in any mass model is the value of $\Upsilon_\star$. Though broad trends in $\Upsilon_\star$ have been measured and modelled (e.g. Bottema 1997; Bell & de Jong 2000a), the precise value for an individual galaxy is not well known, and depends on extinction, star formation history, Initial Mass Function, etc. Rotation curve fitting is a problem with too many free parameters (van Albada & Sancisi 1986; Lake & Feinswog 1989) and some assumptions regarding $\Upsilon_\star$ must be made. We therefore present disk-halo decompositions using four different assumptions for $\Upsilon_\star$ for the galaxies in Sample I. For the galaxies in Sample II only the minimum-disk model is presented.

Minimum disk. This model assumes that the observed rotation curve is due entirely to DM. This gives an upper limit on how concentrated the dark mass component can actually be and is the version of minimum disk preferred in the CDM literature.

Minimum disk + gas. The contribution of the atomic gas (HI and He) is taken into account, but $\Upsilon_\star$ is assumed to be zero. This is the classical definition of minimum disk as used in the HI rotation curve literature.

Constant $\Upsilon_\star$. Here $\Upsilon_\star$ is set equal to a constant value based on an Initial Mass Function and a star formation history appropriate for LSB galaxies. For the range in color $0.4 < B-V < 0.65$ which LSB galaxies normally exhibit (de Blok, van der Hulst & Bothun 1995) a value $\Upsilon_\star(R) = 1.4$ is a good estimate. For example, using the Bruzual & Charlot (1993) model with constant star formation rate and Salpeter IMF, we find that $\Upsilon_\star(R) = 1.4$ corresponds to $B-V = 0.46$. The PEGASE2 model (Rocca-Volmerange, priv. comm.) gives a value $B-V = 0.38$, whereas the model by Cole et al. (2000) yields $B-V = 0.67$. The models by Bell & de Jong (2000b) give values around $B-V \simeq 0.6$. The value $\Upsilon_\star = 1.4$ is thus actually at the "light-weight" end of the plausible range, but this was deliberately chosen in order to give maximum opportunity for the cuspy NFW models to fit the data. We realize that the values derived here should not be regarded as definitive: changes in the IMF model used or different estimates for internal extinction can lead to different values. However, here we attempt to derive a conservative estimate for $\Upsilon_\star$ based on the observed properties of the stellar population. Further (upward) refinement of the $\Upsilon_\star$ value is thus more likely to cause more problems for NFW fits.

Maximum disk. The rotation curve of the stellar component is scaled to the maximum value allowed by the (smooth) rotation curve, but with the restriction that the DM density is required to be positive at all radii (thus

avoiding a so-called "hollow halo") (van Albada & Sancisi 1986). Because of the different DM distributions that we test (core and cusp) this can ocassionally lead to maximum disk values that differ slightly for each of the two models. A more extensive description is given in §6.

Each of the rotation curves was fitted using the GIPSY task ROTMAS. The program determines the best-fitting combination of R_C and V_∞ (for the pseudo-isothermal halo) or c and V_{200} (for the NFW halo), using a least squares fitting routine. We assigned weights to the data points inversely proportional to the square of their uncertainty. Additional checks were made with other fitting programs to check the results of the fits (discussed in Sect. 4.1 below). We also refitted the smooth rotation curves presented in SMT and were able to reproduce the numbers given in their Table 2.

4. RESULTS

Tables 5 and 6 give the results of the model fitting using the NFW halo model. Tables 7 and 8 show the results for the pseudo-isothermal halo. Figure 3 presents the results of the NFW halo and pseudo-isothermal halo mass modelling for each galaxy side-by-side. The two leftmost columns show the results for NFW halo fitting. The two rightmost columns show the pseudo-isothermal halo fitting results.

The first and third columns show the best-fitting models. The rotation curves of the gas are shown as dotted lines, those of the stellar disk component as short-dashed lines. In two cases (U6614 and F571-8) a significant bulge was present which was modelled separately; this is shown as the dot-dashed line (see also Section 4.3). The resulting halo rotation curve is shown as the long-dashed line. The final total model curve is drawn as the full line. In each of the model panels we also give the reduced χ^2 of the fit and the chance p that the data and the model could result from the same parent distribution. This probability was derived using a simple χ^2 test; it is an indicator for the compatibility of the data and the model chosen to describe it. Values $p > 0.95$ indicate that the data and the model are a good match. Values $p < 0.05$ indicate that the model is incompatible with the data, and that better models can be found.

We show two best-fitting values. One as found by the linear fit of the GIPSY ROTMAS task (indicated as a "plus"-cross (+)), and one found by finding the minimum in the plotted logarithmic parameter space (indicated by a "times"-cross (×)). These two are identical, except when extreme parameter values occur (usually during maximum disk fits) and numerical precision of the fitting routine starts to play a role. This effect is visible in the bottom-right corners of the NFW contour plots, where the very large values of V_{200} in combination with the small values of c cause increasingly ragged contours. A large difference between these two best values therefore indicates that the fit should not be regarded as definitive. Indeed, in a number of these cases (indicated in the Tables as italic numbers) the fitting routine was unable to determine a valid solution, and an indicative value had to be chosen by hand. This happened mostly with the NFW models. One of the reasons for this is that the inner parts of the rotation curves can be well described by $V(R) \sim R$, whereas the NFW model has the form $V \sim R^{1/2}$. To accommodate the model, the fit tries to stretch out the NFW curve (resulting in small c and high V_{200}) in order to make it *look* linear.

The second and fourth columns of panels in Fig. 3 show the 1σ (thick contour) and $(2, 3, 4, 5)\sigma$ (thin contours) probability contours of the halo parameters in logarithmic space. The reason for choosing a logarithmic representation is that the χ^2 distributions for the NFW halo parameters often show extended tails towards very small c and/or large V_{200}. For comparison, Fig. 4 shows a representative example of the σ-contours for the minimum disk model of F583-4 plotted in linear c-V_{200} space.

It is important to realize that the σ contours are plotted *with respect to the minimum* χ^2. That is, existence of a narrow distribution only means that the minimum χ^2 is well defined. It does *not* imply that the fit is good in an absolute sense. For that one needs to refer to the value of the reduced χ^2 itself or the probability p that the data and model are compatible. There are many cases where the NFW model is not a good fit, making it difficult to plot absolute likelihood contours.

Finally, in the NFW contour plots in the second column we show the range of c and V_{200} values for the currently popular ΛCDM cosmology as derived from numerical models (Navarro, Frenk & White 1997) (see §5.3). The cross-hatched and single hatched grey areas shows the expected 1σ and 2σ logarithmic scatter in c (where $\sigma_c = 0.18$) as found in numerical models by Bullock et al. (1999). Independent simulations by Jing (1999) find a much smaller logarithmic scatter of $\sigma_c = 0.08$. The latter do of course put much stronger constraints on the NFW results. For the sake of clarity, however, and to give the NFW model as much chance as possible we adopt the larger estimate of the scatter in c of Bullock et al. (1999).

For the pseudo-isothermal halo we show contours of constant central density ρ_0. The contours represent from top to bottom $\rho_0 = 0.1$ (dotted), 1 (dashed), 10, 100, 1000 (dotted) $\times 10^{-3}$ $M_\odot$ pc^{-3}.

4.1. *Weighted versus uniform*

To investigate how stable the derived halo parameters are with respect to the precise definition of the errorbars, we have re-derived the models assigning uniform and equal weights to all data points. Though we do not list the latter values here, we show in Fig. 5 a comparison between the two sets of parameters. It is clear that these agree well, showing that the results presented here are robust against the precise definition of the errorbars.

4.2. *Mass models: smooth and raw*

Has the procedure used to derive the smooth rotation curves affected some of the model results? We established in Sect. 2.4 that this procedure introduced no systematic differences between the smooth curves and the raw data. Here we test this again by checking whether the smooth curves give the same fit results as the raw data.

As the NFW model is more sensitive to changes in the inner slope than the pseudo-isothermal model we will use the former in our checks. We first fit NFW minimum disk models to the smooth and the raw curve of F583-1, as a representation of the data from Paper I. Both fits are

presented in Fig. 6, where we have imposed a minimum error of 4 km s^{-1} on the raw data to make the errorbars consistent with the smooth curve. It is clear that the two fits are identical within the errorbars. Similar results are obtained using other curves from Paper I.

As a second test we evaluate the SMT data. We have fitted several minimum disk NFW models to each of the SMT galaxies. We have fitted the SMT raw data, the smooth curve presented in SMT, and our smooth curve derived from the raw SMT data. These fits were done independently by two of us using independent fit codes on the smoothed (dB) and unsmoothed (McG) data. Table 4 lists the derived parameter values. For comparison, we also list the results for our own independent observation of F568-3 from Paper I. In Fig. 7 we compare the c values derived for each galaxy.

We see that the galaxies for which our smooth curves and the ones presented in SMT agree, also have similar model parameters, which agree with those derived from the raw data (F574-1 and F568-V1). In the other three cases (F563-V2, F568-1, F568-3) the c-values derived from our version of the smooth curves agree with those derived from the raw data, whereas the SMT c-values are higher. It is important to keep in mind that even though the formal fit values show a large discrepancy, the rotation curves themselves only show very subtle differences (Fig. 2). This illustrates the importance of having high-accuracy rotation curves of a large sample. In the following we only consider our smooth versions of the SMT data.

In summary, we believe that the results from our smooth curves are not systematically different from the raw data. As stated before, we prefer to use the smooth curves as these are more evenly sampled, and prevent the occurence of imaginary halo masses which can arise when the occasional (raw) data point happens to scatter below the rotation velocity of the disk alone.

4.3. *Remarks on individual galaxies*

F563-1 For this galaxy independent observations are available from de Blok & Bosma (2001). See Paper I for a comparison. Note that the observed curve differs significantly from the "beam-smearing corrected" model presented in van den Bosch et al. (2000). The model presented there shows an almost flat rotation curve over most of the radial range, which clearly disagrees with the new data. Beam-smearing corrections are not infallible.

F563-V2 This is our version of one of the SMT curves. This curve does significantly worse at fitting NFW than a pseudo-isothermal halo. The systematics seen here are typical for many of the NFW fits: the inner parts are overestimated; the model then underestimates the middle parts, and shoots up again in the outer parts. For this galaxy no R-band photometry is available and we have used B band photometry from McGaugh & Bothun (1994). Assuming $B-R=0.9$, which is the typical color for an LSB, this yields a value for the constant $\Upsilon_\star$ case of $\Upsilon_\star(B)=1.1$. The maximum disk NFW model fits significantly better than the other NFW models. It is however not compatible with cosmological predictions from the numerical models.

F568-1 This is another of the curves presented in SMT. The systematics of overestimating the inner part, underestimating the middle, and overestimating the outer velocities again are also present here. Again maximum disk is the best of the NFW models, which is another way of saying that the shapes of the (inner) rotation curves are more like that expected for the stars (albeit with the wrong $\Upsilon_\star$).

F568-3 This is a well determined curve, for which there are several consistent independent measurements (see Paper I).

F571-8 This is the only edge-on galaxy in Sample I, so we are concerned about optical depth and projection effects in the optical data. (The HI data are not used for this galaxy.) These effects could cause us to measure the rotation velocity at a ring where the optical depth becomes unity. Recently, Matthews & Wood (2000) have used radiative transfer models to investigate optical depth effects on rotation curves in edge-on LSB galaxies, and they conclude that these effect are likely to be small due to the low dust content in LSB galaxies. Bosma et al. (1992), in a comparison of the optical and HI curves of the edge-on galaxy N100, also finds that late-type galaxies tend to be transparant, even when seen edge-on. Nevertheless, we cannot exclude the possibility that the shape of the optical curve is affected. If this is so then *in this case* the mass model will change. For the constant $\Upsilon_\star$ and maximum disk cases we have added an exponential bulge with $\Upsilon_\star(R)_{\rm bulge}=0.5$. See BMH for a description of the bulge-disk decomposition.

F574-1 Another SMT curve. While the pseudo-isothermal halo fits for this galaxy are good, the NFW fits show the by now familiar discrepancy: too steep in the inner part, underestimating the middle, and rising too quickly in the outer parts. Maximum disk NFW provides a good fit, albeit with low c and high $\Upsilon_\star$. F574-1 was the worst case of beam-smearing from the HI sample, but the increase in the initital rate of rise of the rotation curve found optically does not really help NFW. The optical data imply a 'cusp' slope ($\rho\propto r^\alpha$) of $\alpha=-0.49\pm0.26$ (de Blok et al. 2001), still well short of the NFW value $\alpha=-1$. This is the limit in the minimum disk case; if allowance is made for stellar mass, a value even closer to a constant density core is required.

F583-1 A well resolved and well-observed curve that shows the NFW over/under/over-fit discrepancy. For all assumptions about stellar mass, $\chi^2_{\rm ISO}\ll\chi^2_{\rm NFW}$. This galaxy strongly prefers a halo with a constant density core over one with a cusp, a conclusion which has not changed from McGaugh & de Blok (1998). Only a substantial change in the shape of the rotation curve would alter this conclusions, which would require a large *systematic* error. Beam smearing can no longer be invoked as the cause of such a systematic error now that this object has been resolved to sub-kpc scales.

U5750 This curve was observed both by us and de Blok & Bosma (2001), and the two data sets show good agreement (see Paper I). This curve is difficult to model with a standard NFW profile, but the pseudo-isothermal model provides a good fit. The outermost point is taken from the HI curve, and provides an important constraint for the NFW model. Without this point the fit produces $c\sim0$ and an impossibly large V_{200}, a result of the fitting program trying to make $V(R)\sim R^{1/2}$ look like $V\sim R$.

U6614 This is the only giant LSB in Sample I. The anal-

ysis is complicated by the presence of a dominant bulge, which we have modelled as an exponential spherical bulge with $h = 3.0''$ and $\mu_0(R) = 18.4$ mag arcsec^{-2}. The disk has parameters $h = 19''$ and $\mu_0(R) = 21.3$ mag arcsec^{-2}. The rapid rise and subsequent dip in the rotation velocity at small radii clearly suggest the dominance of the bulge in this giant LSB galaxy. We have assumed the bulge to be maximal at $\Upsilon_\star(R) = 3.7$. As the bulge accounts for most of the rotation velocity in the inner parts, this seems to argue against cuspy halos in giant LSB galaxies.

5. DISCUSSION

5.1. *NFW and pseudo-isothermal: a comparison*

The pseudo-isothermal halos generally provide better fits than the NFW halos. In Fig. 8 we compare the reduced χ^2 values for the four different $\Upsilon_\star$ cases. For the minimum disk case we plot Samples I and II, for the other cases only Sample I is plotted. It is clear that the large majority of the curves presented here is best fitted by a pseudo-isothermal halo. This holds true even in the maximum disk case where one might naively expect the dominance of the optical disk to wipe out any discrepancies of a particular halo model (though perhaps not for LSB galaxies).

Another way of comparing the models is given in Table 9. This lists the number of galaxies in Sample I that have good ($p > 0.95$) or bad ($p < 0.05$) fits for each of the two models. Here again it is clear that the pseudo-isothermal model performs much better, for every assumption of $\Upsilon_\star$. These statements do not depend on the errors. If we double (or halve) the size of the error bars, χ^2 will change for both halo cases, but will always remain less for the pseudo-isothermal case. To alter this result would require systematic changes to the shapes of all the rotation curves.

Fig. 9 shows the residuals of the best-fitting minimum disk models versus the observed data. Residuals are plotted against halo scale size (R_{200} for NFW and R_C for pseudo-isothermal halos), radius in kpc, number of optical disk scale lengths and fraction of maximum radius of the rotation curve. As described in the previous section, the NFW fits that fail do so in a systematic way: the inner velocity is overestimated, then the model drops below the observed velocities in the middle and in the outer parts it once again overpredicts the velocity. The NFW residuals are most pronounced when plotted against $R/R_{\rm max}$. The majority of the residuals change sign at $\sim 0.2R_{\rm max}$ and $\sim 0.7R_{\rm max}$. As the radius $R_{\rm max}$ does not have any physical significance, but is determined by the observations (slit angle, presence of Hα, etc.) this indicates that the systematics are due to the choice of model, rather than being associated with any particular length scale in the galaxies. Similar conclusions are reached when the residuals are plotted for the min+gas, constant $\Upsilon_\star$ and maximum disk cases.

Though this is not readily apparent in Fig. 3, the residuals for the pseudo-isothermal halo model also show a systematic behaviour, though at a much lower level than the NFW model. Here the residuals do not increase towards the center, and as the typical size of the residuals is smaller than the uncertainty in the individual data points, this just shows us that the rotation curve shape is subtly different from that of a pure pseudo-isothermal halo. This should come as no surprise given the simplifying assumptions of e.g. minimum disk that we have made.

5.2. *The pseudo-isothermal halo*

Of the two models investigated, the pseudo-isothermal halo best describes the data. Here we briefly explore some correlations between the pseudo-isothermal halo model parameters and the parameters describing the luminous components of the galaxies. To increase the range of the parameters we also consider the samples of Broeils (1992) of (mainly) luminous HSB galaxies, and Swaters (1999) of late-type dwarf galaxies. From these samples we only select bulge-less galaxies brighter than $M_B = -16.5$ to be consistent with the range of luminosities found in our sample.

Fig. 10 presents the results for the three samples. We show the min+gas case, which the two comparison samples refer to as their "minimum disk". The most obvious correlation visible in Fig. 10 is that between R_C and ρ_0. This is a reflection of the fact that these two are correlated through the asymptotic velocity V_∞ (See Eq. 3). Lines of constant V_∞ have a slope of $-\frac{1}{2}$ in the $R_C - \rho_0$ diagram, and the diagram therefore just reflects the limited range in $V_{\rm max}$ in the samples. There is an indication that that R_C increases towards lower surface brightnesses, and that ρ_0 decreases (as one would expect if LSB galaxies inhabited lower density halos).

The large scatter in these figures sheds little light on galaxy formation or the details of pseudo-isothermal halos. How the observed regularities of galaxy kinematics (like the Tully-Fisher relation) can emerge from this scatter remains a mystery.

A further analysis is presented in de Blok et al. (2001) where the mass density distributions that give rise to the observed rotation curves are presented. They show that the minimum disk mass density distributions at small radii can be parametrized by a power law $\rho \sim r^\alpha$ where for the LSB galaxies $\alpha = -0.2 \pm 0.2$, clearly different from $-1.5 \leq \alpha \leq -1$ as predicted by CDM. These minimum disk slopes are upper limits. When stars are properly taken into account, assuming some reasonable value for $\Upsilon_\star$, the slopes decrease, and become even more consistent with constant density cores. Succesfull theories of galaxy formation and evolution that attempt to model LSB galaxies should thus be able to produce halos dominated by constant-density cores.

5.3. *The NFW halo*

As noted earlier, the c and V_{200} halo parameters are related. Here we compare the derived c and V_{200} values with those predicted by ΛCDM with the Navarro, Frenk & White (1997) prescription for $\Omega_m = 0.3$, $\Omega_\Lambda = 0.7$, and $h = 0.65$ with a COBE normalized power spectrum. The values of c depend on the assumed $\Upsilon_\star$, which, as discussed before, is uncertain. Minimum disk however gives strong upper limits on the values of c: when $\Upsilon_\star$ is increased the halo needs to compensate by becoming less concentrated (Navarro, Frenk & White 1997). Minimum disk models with c values higher than found in simulations can usually be reconciled with these observations by increasing $\Upsilon_\star$ or introducing a bulge to bring the c-values down, as

one can see from the progressive decrease in c values from minimum disk to maximum disk.

Explaining minimum disk models with concentrations lower than the simulated values is more difficult. It indicates one or more of three problems: failure of the model, failure of the assumption of circular motion in deriving rotation curves, or a dramatic (non-cosmological) re-distribution of DM. This last option is not really understood, and potentially removes any of the predictive power that the CDM theory has. We will not discuss it here, except to note that the most plausible effect, adiabatic contraction, further concentrates the DM, making the problem worse.

As an aside we note here that the min+gas case sometimes gives slightly higher c-values than the simple minimum disk case. In most cases this is due to a central depression in the HI surface density that gives rises to imaginary rotation velocities, which have to be compensated for by the halo. Also some of the outer rotation velocity is explained by the gas rotation curve, yielding a halo curve that bends more at small radii. Consequently the halo model tends to be slightly more concentrated.

Fig. 11 shows the derived c and V_{200} values and compares them with the ΛCDM predictions. For the minimum disk case we show both Samples I and II, for the other three $\Upsilon_\star$ values only Sample I is shown. The data points are coded to indicate their significance level p.

Several points can be made about Fig.11. Firstly, the bottom-right plot clearly shows that maximum disk is inconsistent with the NFW halos expected to arise in ΛCDM. Secondly, there is some correlation between the significance of the fits and their position in the $c - V_{200}$ diagram. In the minimum disk case the majority (11 out of 14) of the $p > 0.95$ points are found at $V_{200} \lesssim 100$ km s^{-1}. Most (17 out of 19) of the $p < 0.95$ points are found to the right of this line. This division becomes more clear in the minimum disk+gas and constant $\Upsilon_\star$ plots. As the high V_{200} values tend to occur at lower c, this is likely to be the effect of a NFW halo trying to fit a solid-body-like curve, by hiding its curvature outside the visible galaxy, i.e., by decreasing c and increasing V_{200}.

Thirdly, the distribution of points does not agree with that predicted by the numerical models (Jing 1999; Bullock et al. 1999). There are more points above, but more importantly, below the 1σ lines than expected. This low-c tail consists of fits that have a high to reasonable significance p associated with them. We show the distribution again in Fig. 12. The two histograms are for minimum disk (open histogram, Samples I and II) and constant $\Upsilon_\star$ (filled histogram, Sample I). Over-plotted are log-normal distributions showing the distribution derived from numerical simulations. Unfortunately, these simulations do not agree on the value of the dispersion. The ΛCDM model by Bullock et al. (1999) gives a logarithmic dispersion $\sigma_c \simeq 0.18$, while the distribution for relaxed ΛCDM halos as found by Jing (1999) has a logarithmic dispersion of $\sigma_c \simeq 0.08$. The observed distribution is clearly wider than either theoretical one. By changing the cosmology of the model one can change the mean of the distribution (e.g. OCDM has a mean $\log c = 1.25$) (Jing 1999), but the width hardly changes. Thus one can possibly shift the model to higher c to fit the high-c end of the distribution, but it is impossible to explain the large observed low-c tail with the kind of log-normal distribution one derives from the simulations.

5.4. *Morphology*

Rotation curves have the implicit assumption of circular motion. Can non-circular motions affect the rotation curves? As the NFW models show the largest residuals in the centers of some of the LSB galaxies, it is possible that they could be affected by non-circular motions due to non-axisymmetric components. We will investigate the matter here by comparing the morphology of our galaxies with the quality of the fits.

Table 10 contains a short description of the morphology of the galaxies, where we have focussed on the central parts. In the Table "core" refers to a galaxy whose central light distribution can best be described by an axisymmetric model, presumably implying negligible non-circular motions in the inner part. The word "core" is used very loosely here. It does not necessarily indicate the presence of a bulge or massive central component, but is just an indication of the (deprojected) round shape of the isophotes in the inner part of the galaxy. "Bar" indicates a central morphology dominated by a bar-like structure, usually magellanic, that may indicate the presence of non-circular motions.

The results are summarized in Table 11 (for the minimum disk assumption). The conclusion is that there is no clear dependence of residual velocity on morphology. There is thus no indication that the failure of NFW to fit some galaxy rotation curves can be attributed to the presence of bars or non-circular motions.

6. THE MAXIMUM DISK

As noted in the Introduction, the inner rotation curves of HSB galaxies can usually be well explained by scaling up the rotation curve derived from the light distribution. This maximum disk procedure results in $\Upsilon_\star$ values that are reasonably consistent with those derived from stellar population synthesis models (Verheijen 1997; Palunas & Williams 2000; van Albada & Sancisi 1986). Furthermore, bars seem to demand near-maximal disks in HSB galaxies (Debattista & Sellwood 2000; Weiner, Sellwood & Williams 2000)

The matter of maximum disk in LSB galaxies was first discussed by de Blok & McGaugh (1997) who noted that from a stellar population point of view maximum disk demanded unreasonably high $\Upsilon_\star$ values. Substantial amounts of DM were still needed within the optical disk to explain the observed HI curves. SMT revisited the subject and noted that the slightly steeper slopes they found using their Hα curves, enabled them to scale up the disk rotation curve by an even larger factor. The maximum disk $\Upsilon_\star$ value is extremely sensitive to the inner slope, and only a very small increase is needed to change it by a significant factor. In LSB galaxies, the maximum disk $\Upsilon_\star$ values are thus much larger than expected on the basis of colors, metallicities and star formation histories. The higher $\Upsilon_\star$ values as found by SMT worsened this problem (a consequence already noted in de Blok & McGaugh 1997), despite the fact that their maximum disk models could slightly better reproduce the observed inner curve.

Though it seems unlikely that the maximum disk results

can be explained using "reasonable" stellar populations, given what we know about the star formation history, dust content and metallicity of LSB galaxies, the matter is still relevant for exploring possible baryonic disk DM scenarios. To explain maximum disk in LSB galaxies purely in terms of baryons one has to assume a large amount of unseen material in the form of e.g. cold molecular gas, optically thick neutral hydrogen, low mass stars or non-standard initial mass functions. It should be noted though that many of these hypothetical mass components would however violate constraints imposed by disk stability (Athannasoula, Bosma & Papaioannou 1987; Mihos, McGaugh & de Blok 1997), near-infra red colors (Bell et al. 2000; Bell & de Jong 2000a), and would possibly introduce a surface brightness segregation in the baryonic TF-relation (McGaugh et al. 2000)

In Fig. 13 we compare the maximum disk B-band $\Upsilon_\star$ ratios[2] for Sample I, with those derived by Broeils (1992) for a sample of mostly HSB galaxies and by Swaters (1999) for a sample of dwarfs. We again show only bulge-less galaxies brighter than $M_B = -16.5$. Also indicated are $\Upsilon_\star$ values from Bell & de Jong (2000b), who tabulate stellar mass-to-light ratios for various star formation histories and population synthesis models as a function of color. Here we show representative values (assuming a simple Salpeter IMF) spanning the color range exhibited by late-type HSB galaxies, gas-rich dwarfs and LSB galaxies.

The $\Upsilon_\star$ values for HSB galaxies agree to within a factor of 3 and can be considered to be (close to) maximum disk. The values found for LSB galaxies and dwarfs are less easily reconciled with the model values. Observationally values up to $\Upsilon_\star(B) = 15$ are found, while the typical model value (again for a simple Salpeter IMF) is $\Upsilon_\star(B) \simeq 0.9$ for $B-R = 0.8$ (the average color for a dwarf/LSB). This discrepancy cannot be explained with extinction or population effects. Extinction in dwarfs and LSB galaxies is less than in HSB galaxies (Tully & Verheijen 1998), and a factor of ~ 17 (3.0 mag) extinction is hard to reconcile with the known properties of LSB galaxies. Line-of-sight extinctions observed towards HII regions in LSB galaxies are never as large (McGaugh 1994; de Blok & van der Hulst 1998).

Apart from changing the IMF in an *ad hoc* way it is hard to see how such high $\Upsilon_\star$ values can be reached given the constraints imposed by what we know about the star formation history (low SFR in past and at present) and the blue (optical and NIR) colors of LSB galaxies (de Blok, van der Hulst & Bothun 1995; McGaugh & Bothun 1994; van den Hoek et al. 2000; Bell et al. 2000; Bell & de Jong 2000a; de Jong 1996). It is likely that the maximum disk values as found in LSB galaxies are not representative of the evolutionary stage of these galaxies. While the maximum disk prescription now has somewhat greater success in predicting the inner shape of the rotation curves of LSB galaxies, it requires stellar mass-to-light ratios which are too large for the stellar populations in these galaxies. The mass discrepancies are still large; all this does is move the DM from halo to disk.

6.1. *The maximum surface density of a disk*

Just as the minimum disk assumption gives us an upper limit on the amount of DM implied by rotation curves, the maximum disk hypothesis gives us an upper limit on the amount of mass that could potentially be hidden in a disk. It is therefore still useful to ask ourselves what these maximum disk upper limits imply for the stellar disks.

Maximum disk means maximum surface density (luminous surface density times $\Upsilon_\star$), and therefore gives an absolute upper limit on the mass surface density in stellar disks (for mass components that are distributed like the stars). Figure 14 summarizes the maximum disk results for the Sample I LSB galaxies as well as the Broeils (1992) and Swaters (1999) HSB and dwarf samples. We plot the maximum disk $\Upsilon_\star$ values, as well as the luminosity, rotation velocity, surface brightness, and maximum disk surface density. The data are divided into three surface brightness bins. As already shown in de Blok & McGaugh (1997), at fixed $V_{\rm max}$ LSB galaxies have higher maximum $\Upsilon_\star$ values than HSB galaxies.

Figure 14 also shows the maximum surface density σ. As the decrease in surface brightness is faster than the increase in maximum disk $\Upsilon_\star$, towards low surface brightnesses the maximum surface density σ in a disk decreases with surface brightness. The $\mu_0 - \sigma$ panel suggests that there is a well-defined upper limit to the maximum surface density disks can attain. Even under maximum disk, LSB galaxy disks have on average lower surface densities than HSB galaxy disks, again putting limits on the amount of baryonic mass one can hide in these disk.

Figure 3 shows that even in the maximum disk case most LSB galaxies have $V_{\rm max}({\rm disk}) < V_{\rm max}({\rm observed})$. Therefore, even in the maximum disk case a moderate amount of DM is still required in the optical disk. It is therefore hard to explain the TF relation for LSB galaxies in the context of maximum disk: the stellar disk then needs to provide the luminosity, *and* the necessary rotation velocity. LSB galaxies would deviate systematically from the HSB TF relation, which is evidently not the case (Zwaan et al. 1995).

This is illustrated in the inset panel in Fig. 14 (lower-right). Using the arguments in Zwaan et al. (1995) we find that $\Sigma_0(\Upsilon)^2$ needs to be constant for galaxies to obey a TF relation independent of surface brightness. If all galaxies were truly maximum disk (in the sense that $V_{\rm max}({\rm disk}) \simeq V_{\rm max}({\rm observed})$, one could replace this by the requirement that $\Sigma_0(\Upsilon_\star)^2_{\rm max}$ needs to be constant. The lower-right panel shows that this is not the case: at fixed $V_{\rm max}$ there is a substantial scatter which would translate in ~ 5 mag scatter in TF. Clearly the observed scatter is much smaller, and this shows the clear need for an additional mass component to make TF work. In other words, maximum disk for *all* galaxies and TF are incompatible.

7. CONCLUSIONS

The most important conclusion from this work is that the large majority of the high-resolution rotation curves presented here prefer the pseudo-isothermal core-dominated halo model. For a small number of galaxies

[2] These were derived by converting our R-band values using the $B-R$ color. We converted our data to B-band, rather than converting the HSB data to R-band, as the colors of LSB galaxies are better determined than those of the Broeils HSB galaxies. The color gradients in LSB galaxies are small, so systematic effects are negligible.

neither the pseudo-isothermal nor the NFW models are an adequate description of the data. This should not come as a surprise as the true DM distribution is likely to be more complex than the models presented here. Nevertheless, the general trend is that for almost all galaxies discussed here the relative quality of the fits using the pseudo-isothermal model is better than those for the NFW model.

For a small numer of galaxies the NFW model provides a good fit, but generally the concentrations derived from the observed rotation curves are lower than predicted by the simulations. This is hard to fix: the most likely effect which may alter the initial cosmological NFW halo is adiabatic contraction, but this has the effect of making the final (observed) halo *more* concentrated, so one would have to start off with (cosmologically relevant) halos that are even *less* concentrated.

It is worrying that for one or two extreme cases the difference between "CDM does work" or "CDM doesn't work" depends on subtle differences in data, data handling, or analysis. Figure 7 illustrates that opposite claims can sometimes be made from the same data. Hence we reiterate the need for the highest quality data of a large sample, in order to minimize these effects.

We refer to de Blok et al. (2001) where it is shown that *all* data presented here are consistent with a core-dominated model; the good NFW fits that are found for a number of LSB galaxies can be attributed to resolution effects.

We summarize our results as follows.

- Pseudo-Isothermal halos are a better description of the data than NFW halos.
- The number of galaxies that cannot be fit with NFW halos is significantly larger than the number of galaxies that cannot be fitted with the pseudo-isothermal model.
- The quality of the fit is not obviously related to morphology, luminosity, or surface brightness.
- A larger number of low-c NFW halos is found than one would expect based on the distribution derived from CDM simulations.
- If one were to construct models that would have the correct c-V_{200} values as predicted by cosmology, then the resulting $\Upsilon_\star$ values would be too low to be consistent with stellar population numbers. The shape of the curves would still be wrong.
- The maximum disk prescription works to predict the inner rotation curve shape to some extent, but gives mass-to-light ratios which are too high to be accounted for by stellar population synthesis models.
- Applying the maximum disk values yields absolute upper limits on the disk mass surface density that is strongly correlated with surface brightness.

We thank Roelof Bottema and Rob Swaters for their helpful comments on early drafts of this paper. We thank the anonymous referee for a thorough examination of the data. The work of SSM is supported in part by NSF grant AST9901663. This research has made use of the NASA/IPAC Extragalactic Database (NED) which is operated by the Jet Propulsion Laboratory, California Institute of Technology, under contract with the National Aeronautics and Space Administration. This research has made use of NASA's Astrophysics Data System Abstract Service.

REFERENCES

Athannasoula, E., Bosma, A., Papaioannou, S., 1987, A&A, 179, 23
Begeman, K., 1987, PhD Thesis, University of Groningen
Bell, E.F., de Jong, R.S., 2000, MNRAS, 312, 497
Bell, E. F., & de Jong, R. S. 2001, ApJ, submitted
Bell, E.F., Barnaby, D., Bower, R.G., de Jong, R.S., Harper, D.A., Hereld, M., Loewenstein, R.F., Rauscher, B.J., 2000, MNRAS, 312, 470
Blais-Ouellette, S., Amram, P., Carignan, C., 2001, AJ, in press (astro-ph/0006449)
Bosma A., Byun Y., Freeman K.C., Athanassoula E., 1992, ApJ, 400, 21
Bothun G.D., Impey C.D., McGaugh S.S., 1997, PASP, 109, 745
Bottema, R., 1997, A&A, 328, 517
Broeils, A.H., 1992, PhD Thesis, University of Groningen
Bruzual, A.G., Charlot, S, ApJ, 405, 538
Bullock, J.S., Kolatt, T.S., Sigad, Y., Somerville, R.S., Kravtsov, A.V., Klypin, A.A., Primack, J.R., & Dekel, A. 1999 (astro-ph/9908159), MNRAS, submitted
Casertano, S. 1983, MNRAS, 203, 735
Cole, S., Lacey, C.G., Baugh, C.M., Frenk, C.S., 2000 (astro-ph/0007281), MNRAS, in press
Côté, S., Carignan, C. & Freeman, K.C. 2000, AJ, 120, 3027
de Blok W.J.G., van der Hulst J.M., 1998, A&A, 335, 421
de Blok W.J.G., van der Hulst J.M., Bothun G.D., 1995, MNRAS, 274, 235
de Blok, W.J.G., McGaugh, S.S. 1996, ApJ, 469, L89
de Blok, W.J.G., McGaugh, S.S, Bosma, A., Rubin, V., 2001, ApJ, in press
de Blok W.J.G., McGaugh S.S., van der Hulst J.M., 1996, MNRAS, 283, 18
de Blok, W.J.G., McGaugh, S.S., 1997, MNRAS, 290, 533
de Jong, R.S., 1996, A&A, 313, 377
Debattista, V.P., Sellwood, J.A., 2000 (astro-ph/0006275)
Flores, R.A., Primack, J.R., 1994, ApJ, 427, L1
Freeman K.C., 1970, ApJ, 160, 811
Jing, Y.P. 1999 (astro-ph/9901340)
Lake, G., Feinswog, L. 1989, AJ, 98, 166
Loader, C., 1999, *Local Regression and Likelihood*, Springer-Verlag: New York
Mac Low, M.-M., Ferrara, A., 1998, ApJ, 513, 142
Mateo, M.L., 1998, ARA&A, 36, 435
Matthews, L.D., Wood, K., 2000, astro-ph/0010033
McGaugh S.S., 1994, ApJ, 426, 135
McGaugh S.S., Bothun G.D., 1994, AJ, 107, 530
McGaugh, S.S., de Blok, W.J.G., 1997, ApJ, 481, 689
McGaugh, S.S., de Blok, W.J.G., 1998, ApJ, 499, 41
McGaugh, S.S., Rubin, V., de Blok, W.J.G., 2000, ApJ, submitted
McGaugh, S.S., Schombert, J.M., Bothun, G.D., de Blok, W.J.G., 2000, ApJ, 533, L99
Mihos, J.C., McGaugh, S.S., de Blok, W.J.G., 1997, ApJ, 477, L79
Moore, B. 1994, Nature, 370, 629
Moore, B., Quinn, T., Governato, F., Stadel, J., Lake, G., 1999, MNRAS, 310, 1147
Navarro, J.F., Frenk, C.S., White, S.D.M. 1996, ApJ, 462, 563
Navarro, J.F., Frenk, C.S., & White, S.D.M. 1997, ApJ, 490, 493
Palunas, P., Williams, T.B., 2000 (astro-ph/0009161)
Persic M., Salucci P., Stel., F., 1996, MNRAS, 281, 27
Pickering, T.E., Impey, C.D., van Gorkom, J.H., Bothun, G.D., 1997, AJ, 114, 1858
Sprayberry D., Impey C.D., Bothun G.D., Irwin M., 1995, AJ109, 558
Swaters, R.A., 1999, PhD Thesis, University of Groningen
Swaters, R.A., Madore, B.F., Trewhella, M., 2000, ApJ, 531, L107
Tully, R.B., Verheijen, M.A.W., 1997, ApJ, 484, 145

van Albada, T.S, Sancisi, R., 1986, Phil. Trans. R. Soc. Lond. A, 320, 447
van den Bosch, F.C., Robertson, B.E., Dalcanton, J.J., de Blok, W.J.G., 2000, AJ, 119, 1579
van den Hoek, L.B., de Blok, W.J.G., van der Hulst, J.M., de Jong, T., 2000, A&A, 357, 397
van der Hulst J.M., Skillman E.D., Smith T.R., Bothun G.D., McGaugh S.S., de Blok W.J.G., 1993, AJ, 106, 548
van der Kruit, P.C., & Searle, L. 1981, A&A, 95, 105
Verheijen, M.A.W., PhD Thesis, University of Groningen
Weiner, B.J., Sellwood, J.A., Williams, T.B., 2000 (astro-ph/0008205)
Zwaan M.A., van der Hulst J.M., de Blok W.J.G., McGaugh S.S., 1995, MNRAS273, L35

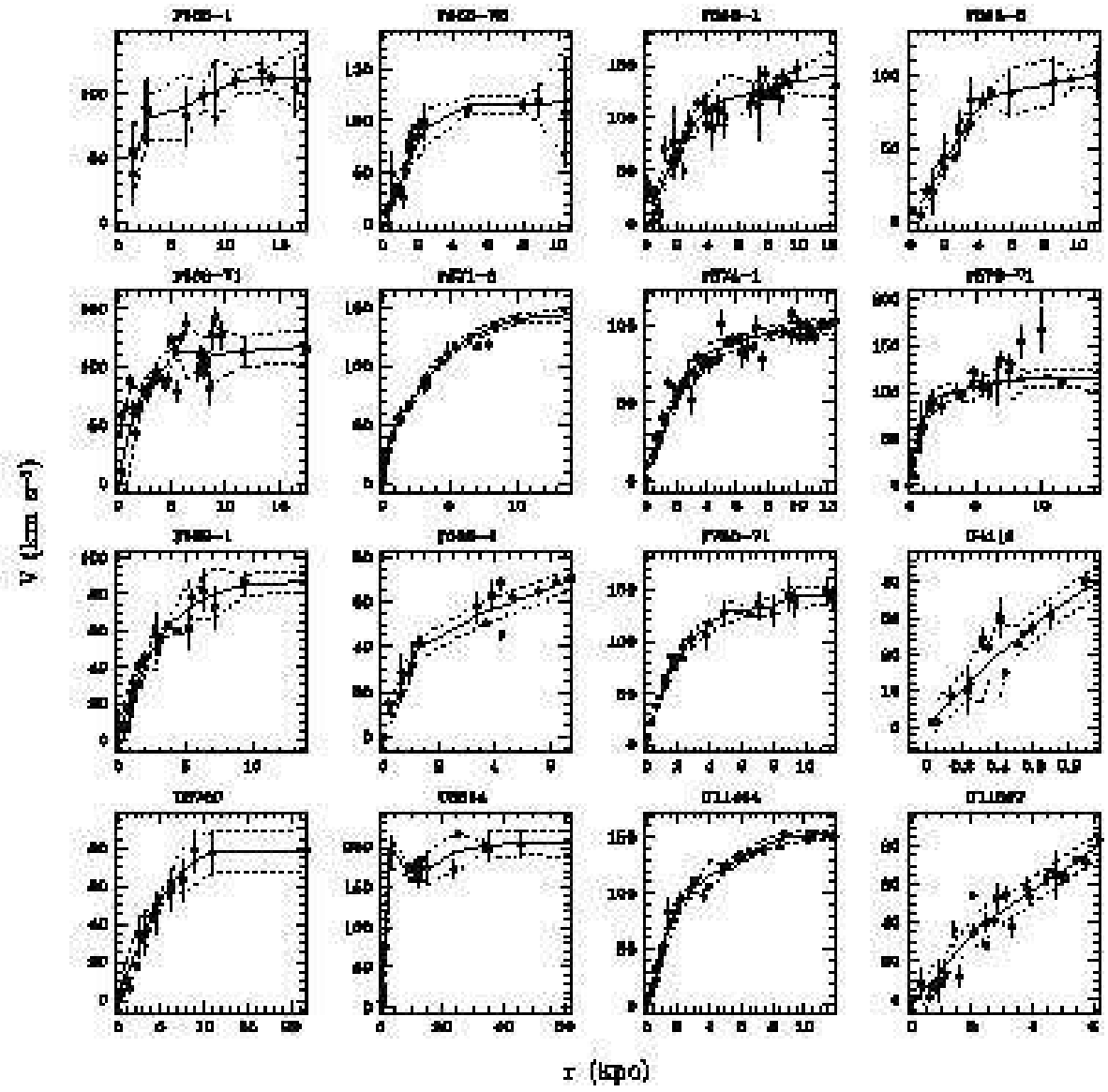

FIG. 1.— Comparison of the raw hybrid rotation curves (black dots) with the smooth curves (full lines). The derived uncertainties in the smooth curves are indicated by the dotted lines.

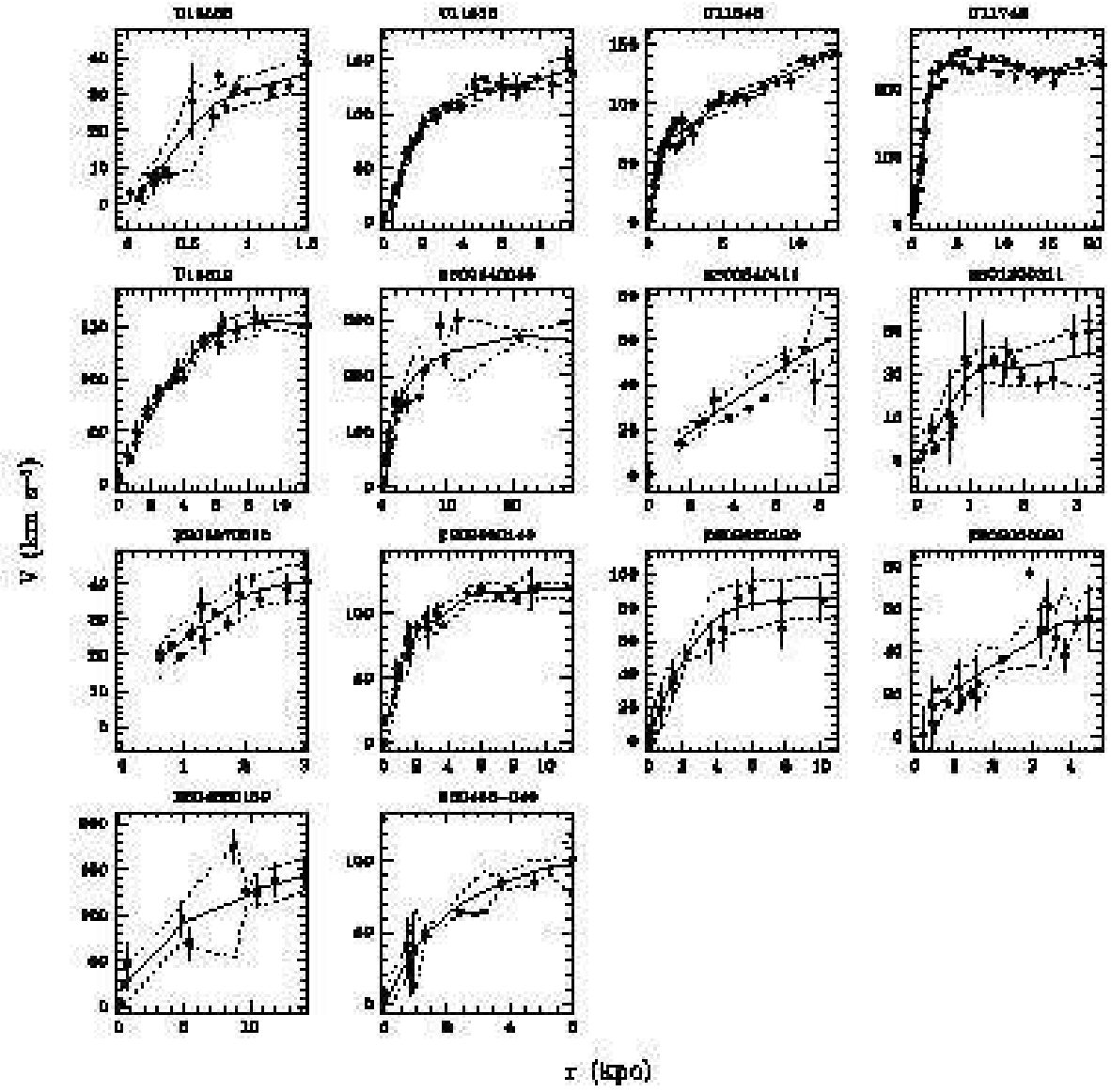

FIG. 1.— CONTINUED

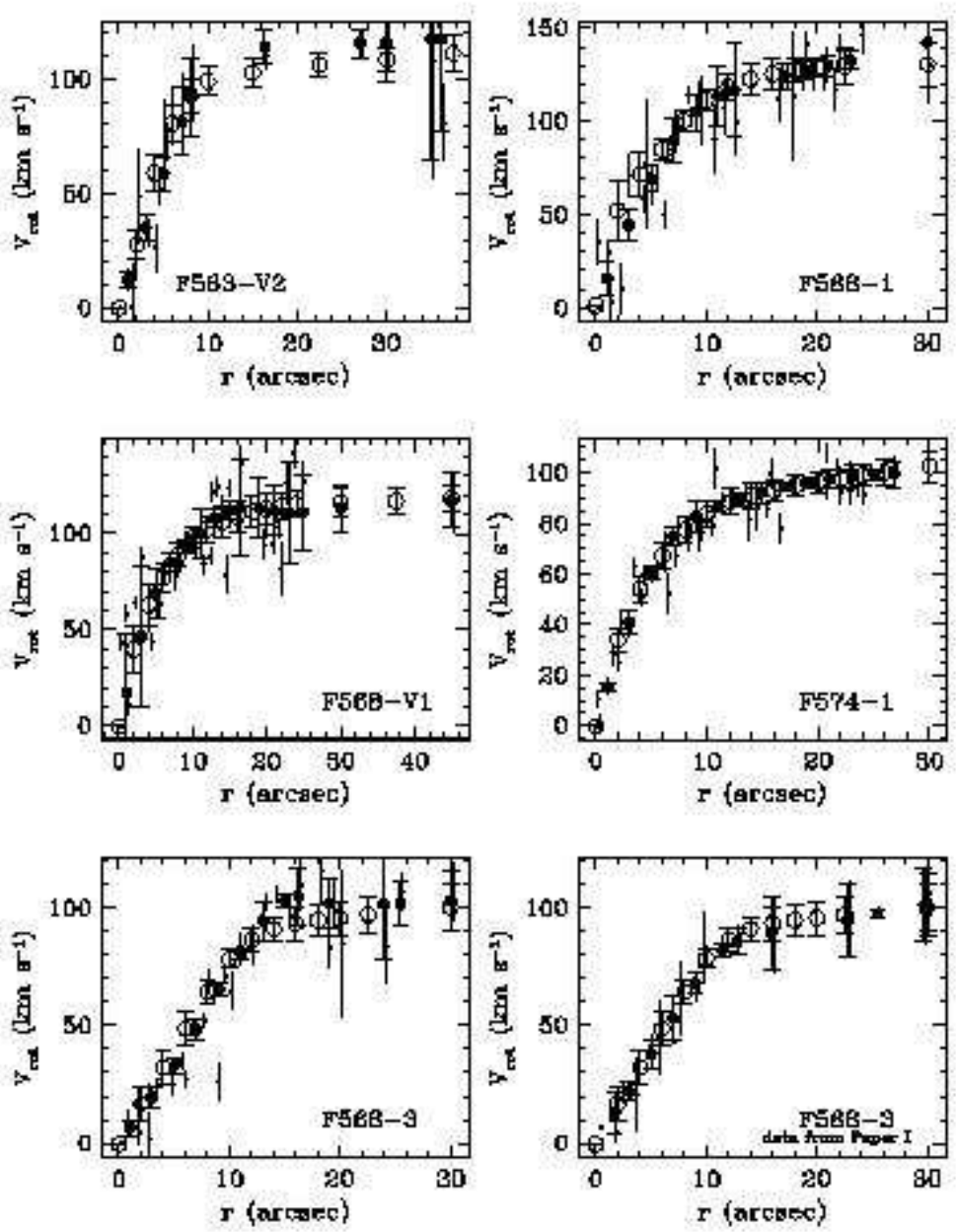

FIG. 2.— Comparison of our analysis of the STM data with their resampled rotation curves. The top four panels and the bottom left panel show the raw data from STM (grey small dots), their resampled and smoothed rotation curves (open circles), and our local regression fits to the same data (filled large circles). The raw data have been offset by $+0.2''$ to avoid overlap with the binned data. The bottom right panel shows the raw data for F568-3 taken from Paper I, along with the STM model (identical to the model shown in the bottom-left panel) and our resampled rotation curve based on the data from Paper I. Small differences between the various curves are discussed in the text.

FIG. 3.— Mass models assuming NFW halo (left) and pseudo-isothermal halo (right). Within each panel the left column shows the best fitting model, the right column shows the probability distribution of the halo parameters. For a full description see text (Sect. 4). **Figure 3 not available due to size limitations. All figures available at http://www.atnf.csiro.au/∼edeblok/papers/deblok.ps.gz**

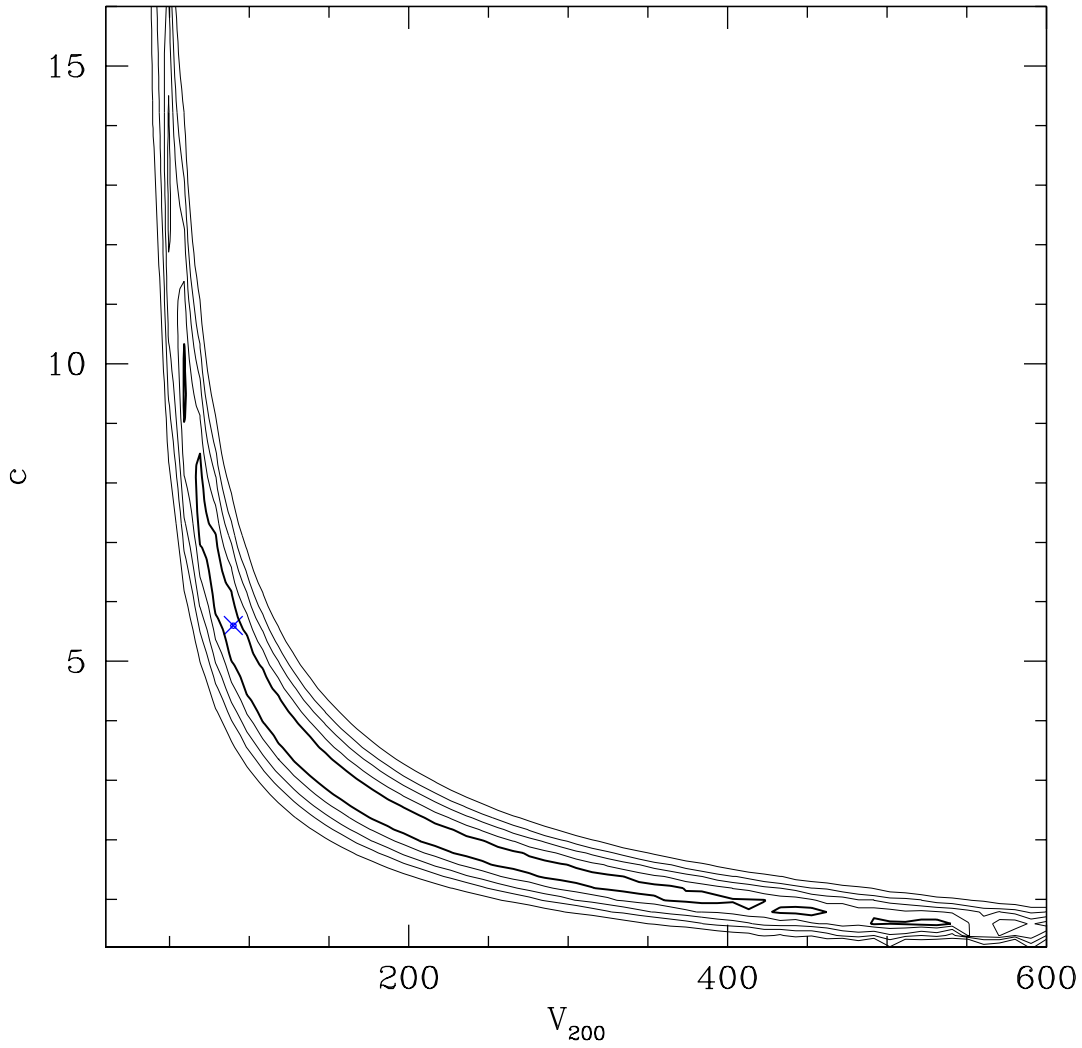

FIG. 4.— The error contours for the minimum disk NFW fit of F583-4 drawn in linear $c - V_{200}$ space. Contour values are as in Fig. 3.

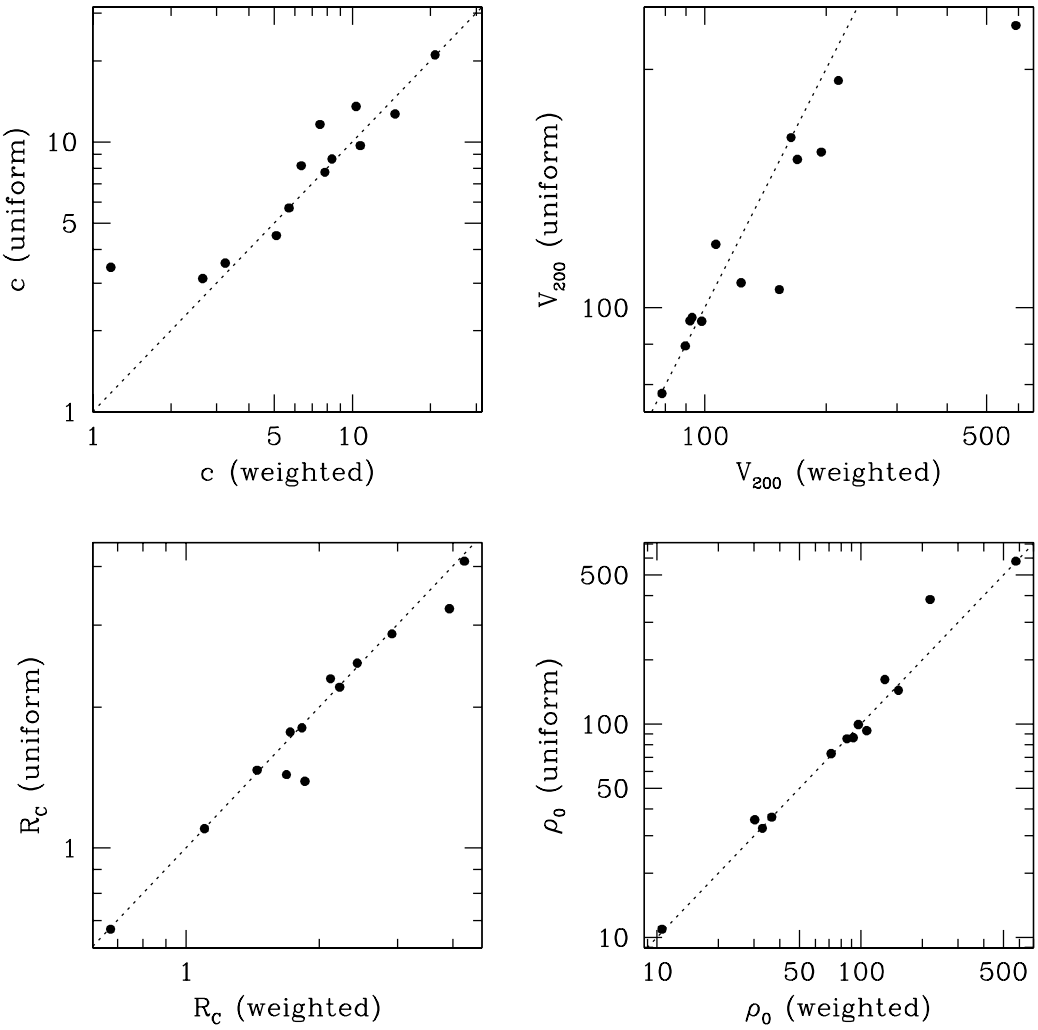

FIG. 5.— Comparison of the NFW halo parameters c and V_{200} and the pseudo-isothermal halo parameters R_C and ρ_0, as derived using a weighted model fit, using the inverse variance as weight, and uniform errorbars. There is good agreement. The somewhat increased scatter at extreme values is not significant, as the shape of the model in that area of parameter space is fairly insensitive to the precise values.

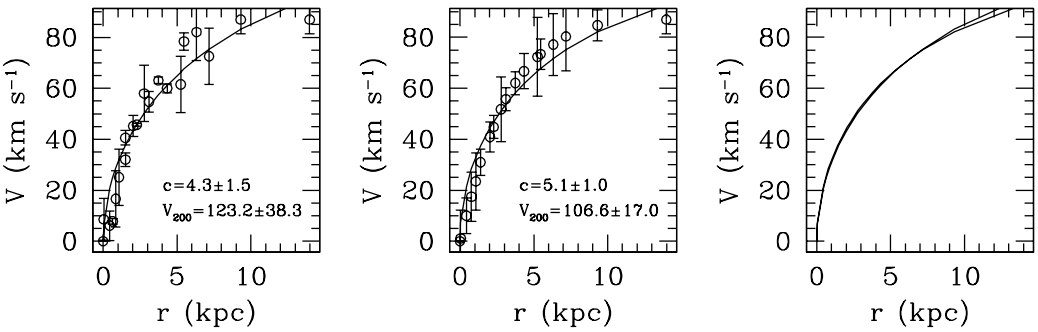

FIG. 6.— Comparison of NFW minimum disk fits to the raw rotation curve of F583-1 (left panel) and the smooth curve (middle panel). The right panel compares the two fits, which are virtually identical. The fit parameters shown in the panels agree within their errors.

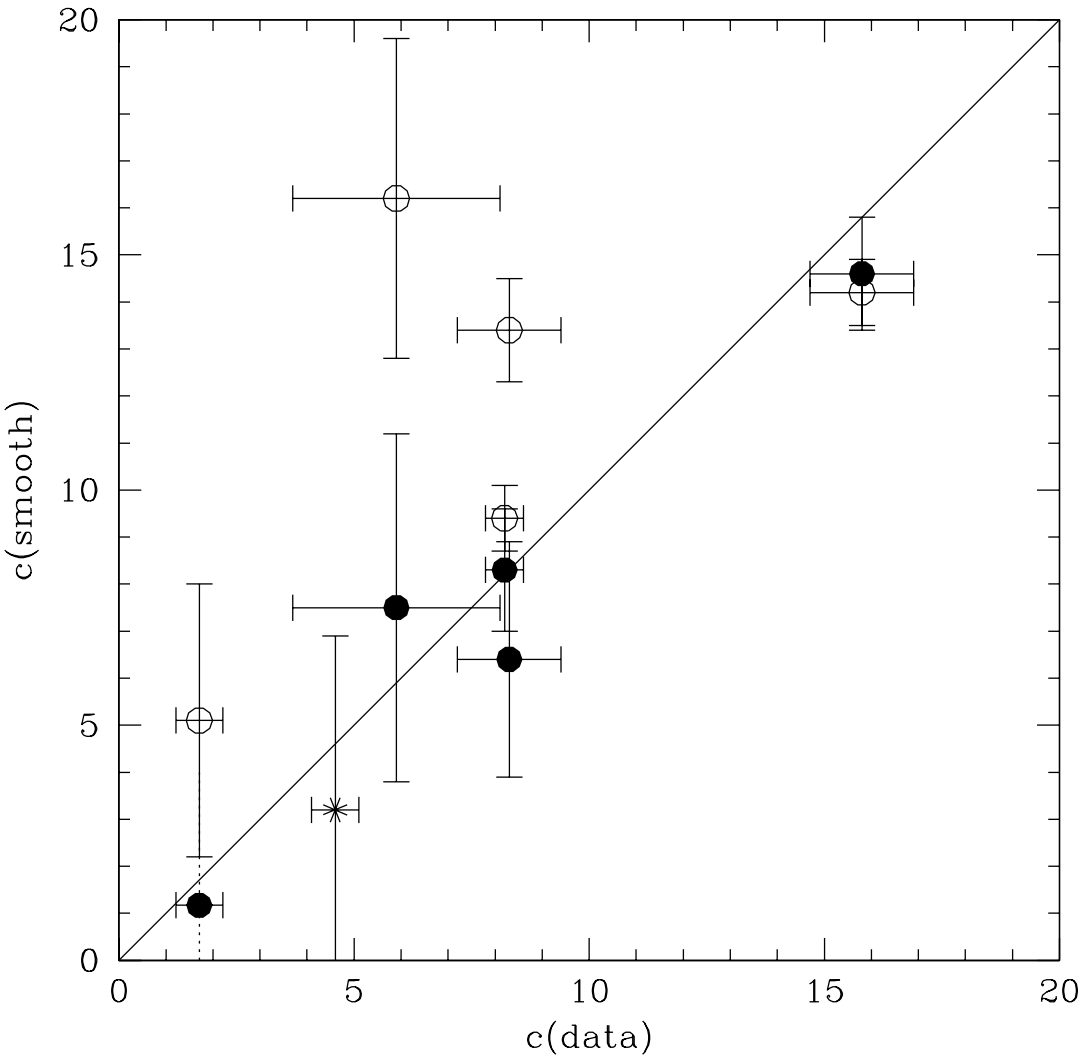

FIG. 7.— Comparison of the NFW halo parameter c fitted to the SMT data. The horizontal axis represents c-values derived from the raw data; the vertical axis those derived from the smooth curves. The open symbols compare the values derived from the raw data with those derived from the SMT smooth curves. The filled symbols compare the raw data results with the values derived from our smooth curves. The star symbol represents the result from our analysis of our data for F568-3. The dotted line in the lower-left corner indicates that no realistic errorbars could be derived for this fit. Our analysis of the raw, unsmoothed data, of our smoothed versions of these curves, and of the SMT smooth curves show good agreement. The only exceptions are F563-V2 and F568-1, for which the SMT curves give larger concentrations. While the formal fits differ significantly in these cases, the differences in the curves being fit are subtle (see Fig. 2). This illustrates the importance of high accuracy data.

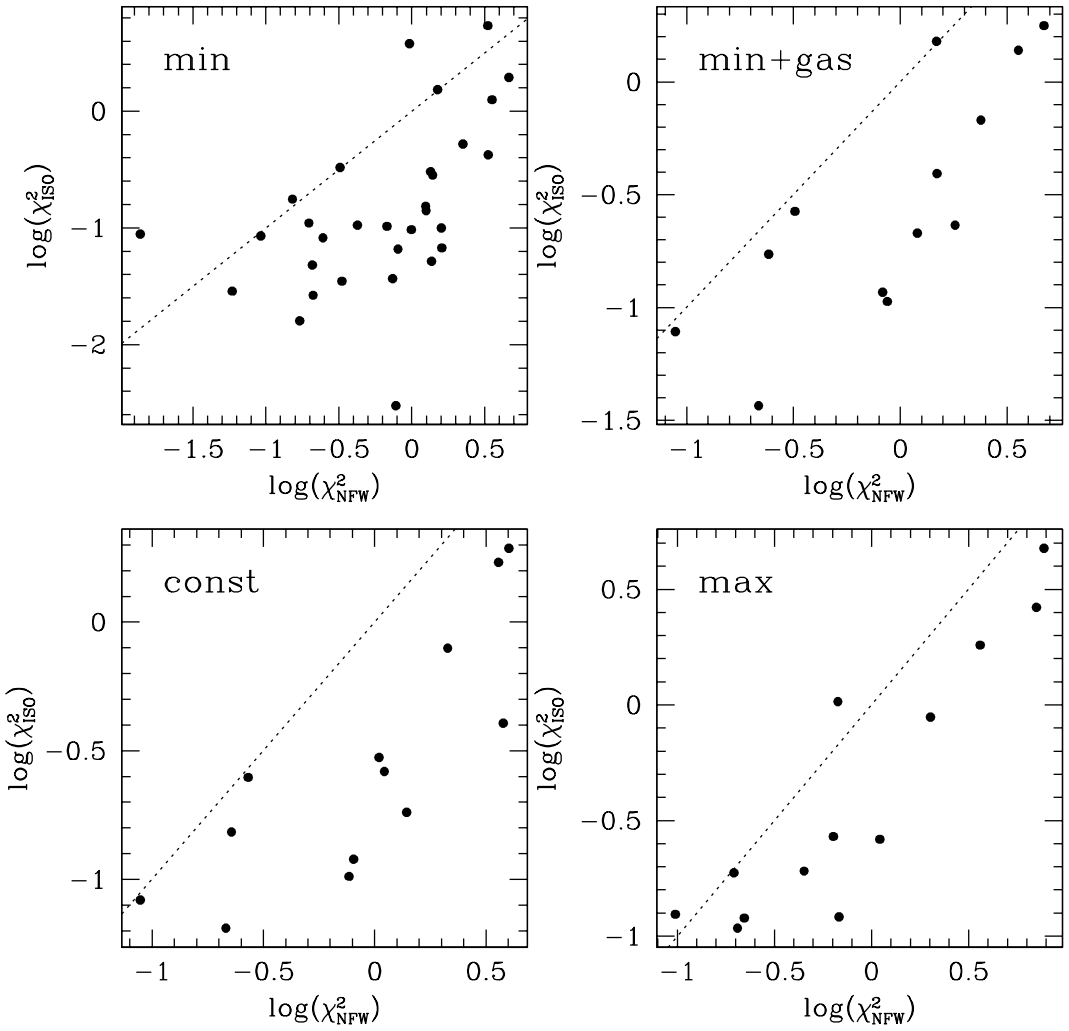

FIG. 8.— Comparison of the reduced $\chi 2$ values using NFW and ISO halos, using the four assumptions for $\Upsilon_\star$ as described in the text. Note that the axes have logarithmic scales. The dotted lines are lines of equality.

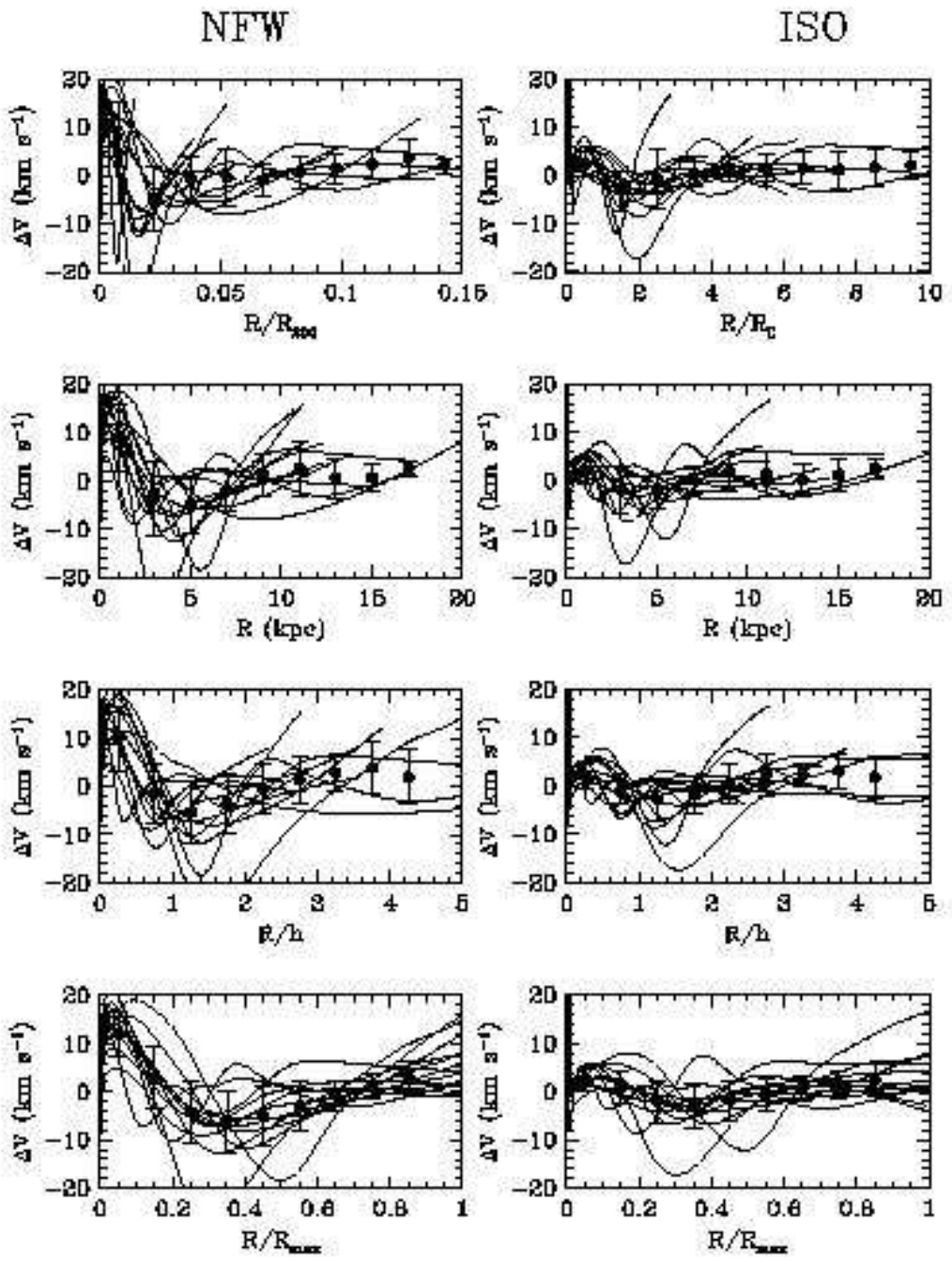

FIG. 9.— Comparison of the residuals $\Delta V = V_{model} - V_{obs}$ for Sample I (minimum disk), plotted against number of halo scale radii (first row), absolute radius (second row), number of optical disk scale lengths (third row) and fraction of maximum radius of rotation curve (fourth row). The left panels show residuals using NFW halo models, the right panels show the pseudo-isothermal halo case. Also shown are the average residuals and standard deviations (filled dots). The residuals at small radii are much larger for the NFW model than for the ISO model. The low-level systematic residuals that are also apparent for the pseudo-isothermal halo, probably tell us that real halos are subtly different from pseudo-isothermal.

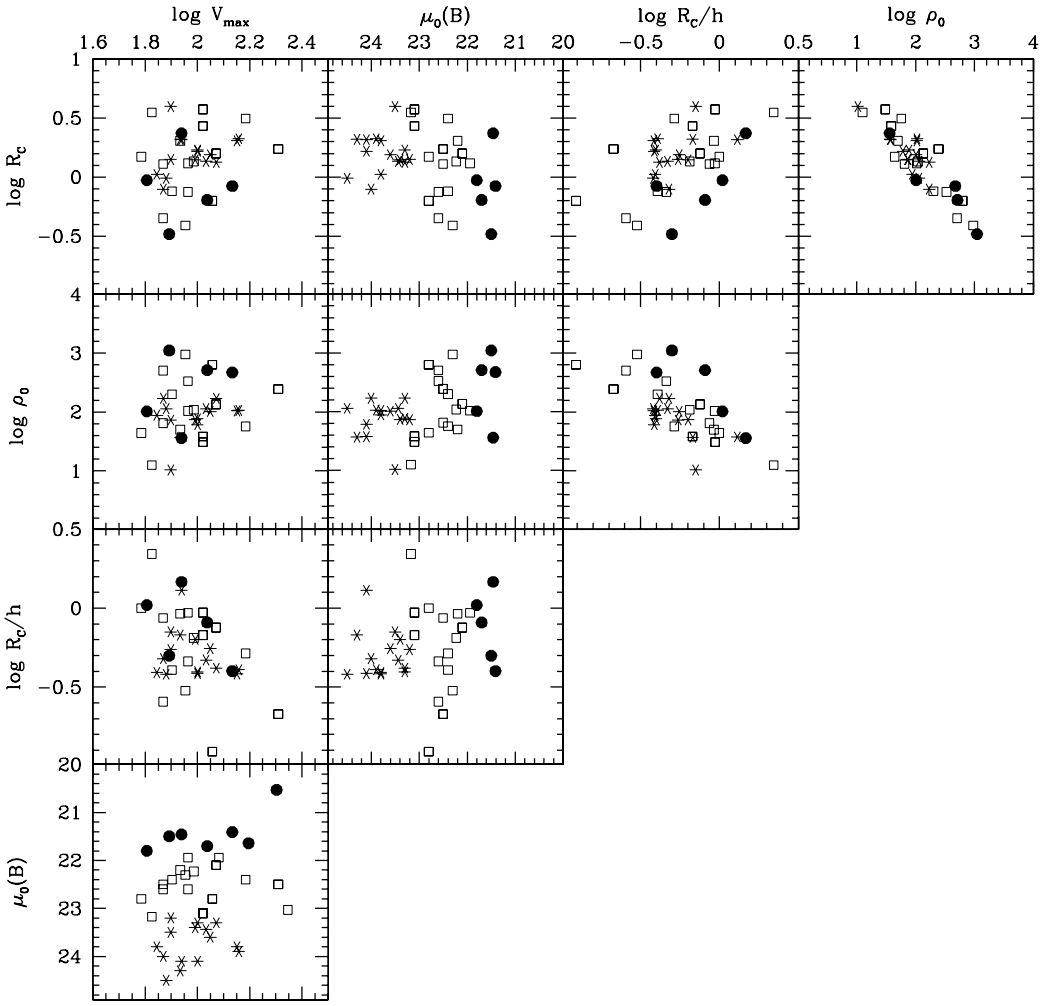

FIG. 10.— Correlations involving pseudo-isothermal halo parameters assuming minimum disk+gas. Shown are maximum rotation velocity $V_{\rm max}$ [km s^{-1}], surface brightness $\mu_0[B$-mag arcsec$^{-2}]$, central halo density ρ_0 [10^{-3} $M_\odot$ pc^{-3}], halo core radius R_C [kpc], and the ratio of core radius and optical disk scale length R_C/h. Included are the bulge-less HSB galaxies brighter than $M_B = -16.5$ from Broeils (1992) and the high-quality ($q = 0$ or 1) curves of bright $M_B < -16.5$ dwarfs from Swaters (1999). Black circles: $\mu_0(B) < 21.9$ mag arcsec^{-2}; open squares: $21.9 \leq \mu_0(B) \leq 23.2$; stars: $\mu_0(B) > 23.2$ mag arcsec^{-2}. See text for details.

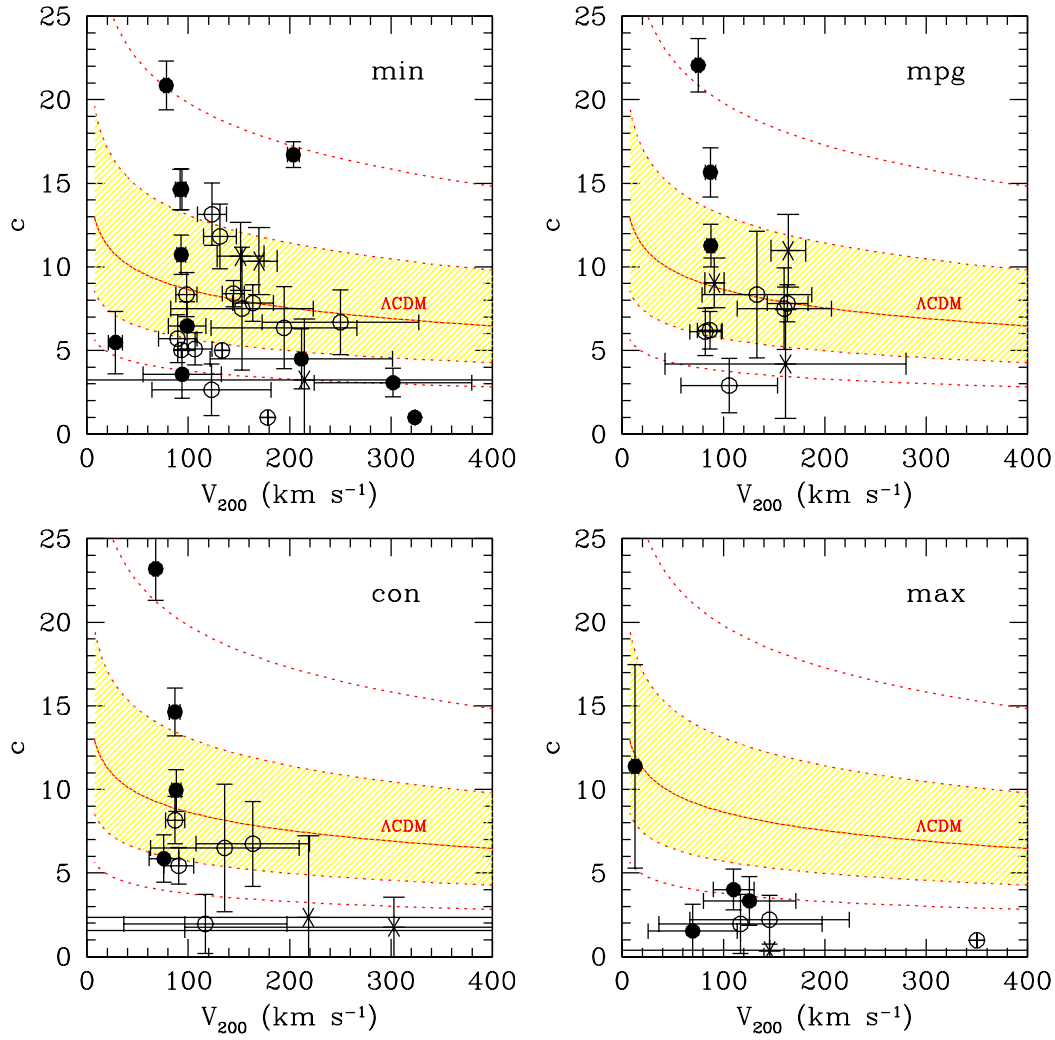

FIG. 11.— The NFW halo concentration parameter c plotted against the halo rotation velocity V_{200} for the four different $\Upsilon_\star$ cases discussed in this paper. Black dots represent good fits ($p > 0.95$), open dots average quality fits ($0.05 < p < 0.95$). Crosses represent bad fits ($p < 0.05$). Good fits are primarily found at $V_{200} < 100$ km s^{-1}. Maximum disk is clearly inconsistent with NFW. The line labeled "ΛCDM" shows the prediction for that cosmology derived from numerical models. The grey area encloses the 1σ uncertainty (Bullock et al. 1999). The upper and lower dotted line show the 2σ uncertainty. The minimum disk panel shows both Samples I and II. The other three panels only show Sample I.

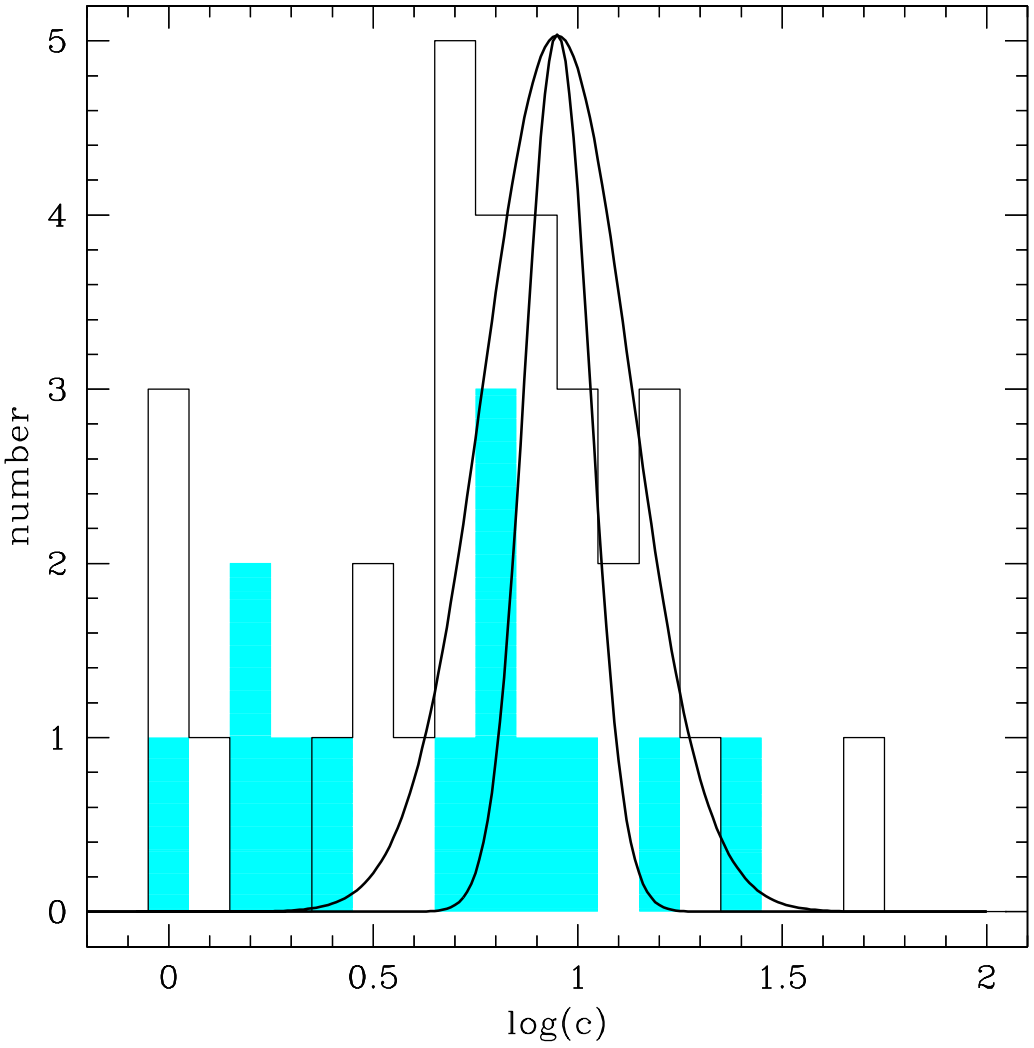

FIG. 12.— Distribution of the c-parameter for the minimum disk case (open histogram) and the constant $\Upsilon_\star$ case (solid histogram). Overplotted is the theoretical log-normal distribution for a ΛCDM cosmology, derived from independent numerical simulations by Jing (1999) and Bullock et al. (1999). The former finds a log-normal distribution with a logarithmic dispersion $\sigma_c = 0.08$. The latter finds a wider log-normal distribution with $\sigma_c = 0.18$. The observed low-c tail is not consistent with either theoretical distribution. The theoretical distributions have been arbitrarily normalized to coincide with the maximum of the observed distribution.

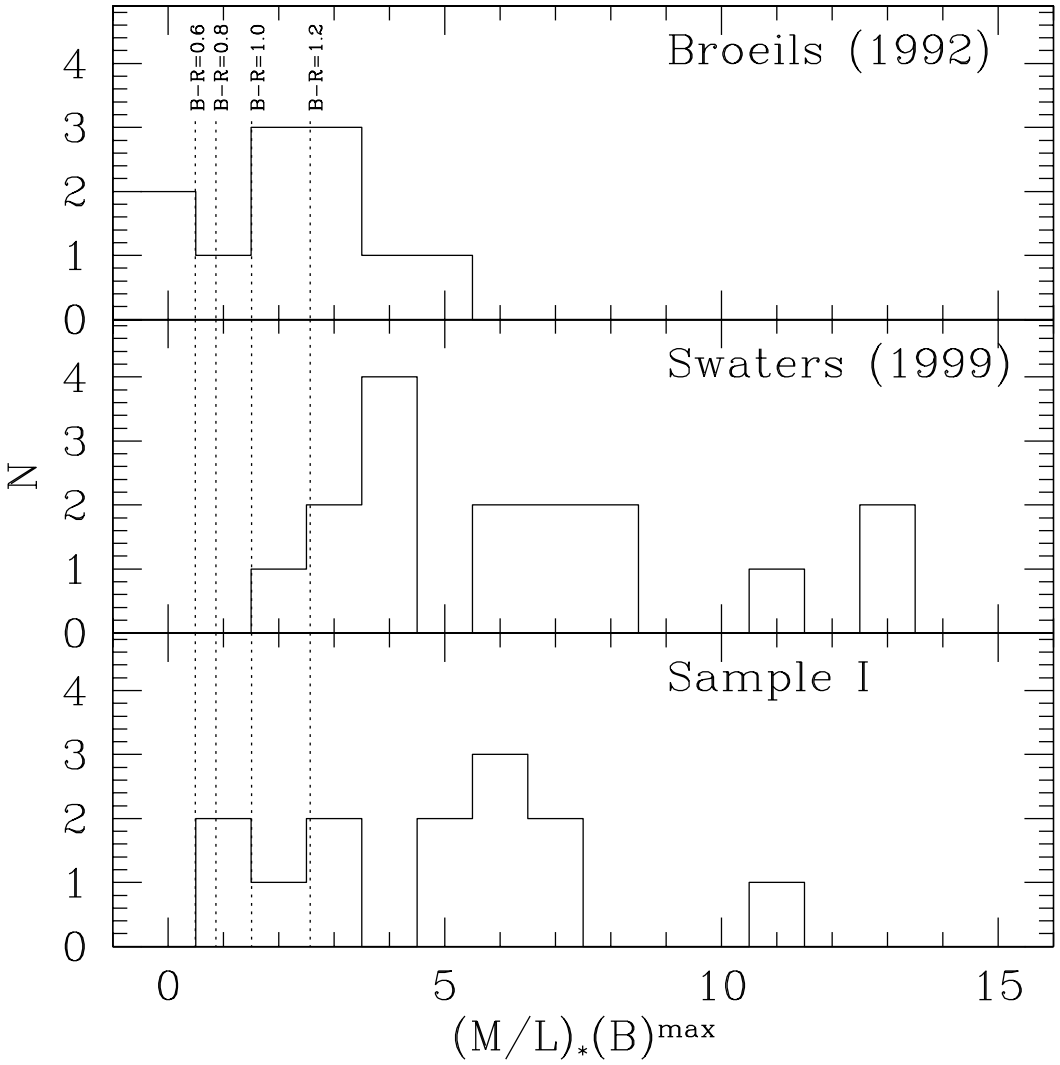

FIG. 13.— Histograms of the maximum disk $\Upsilon_\star$ values. The top panel refers to bulge-less galaxies from the collection of Broeils (1992) brighter than $M_B = -16.5$. The middle panel refers to dwarf galaxies brighter than $M_B = -16.5$ from Swaters (1999) with quality index 0 or 1 (very good to good). The bottom panel shows Sample I. Also indicated are the values for $\Upsilon_\star$ using population synthesis models by Bell & de Jong (2001) assuming a simple Salpeter IMF.

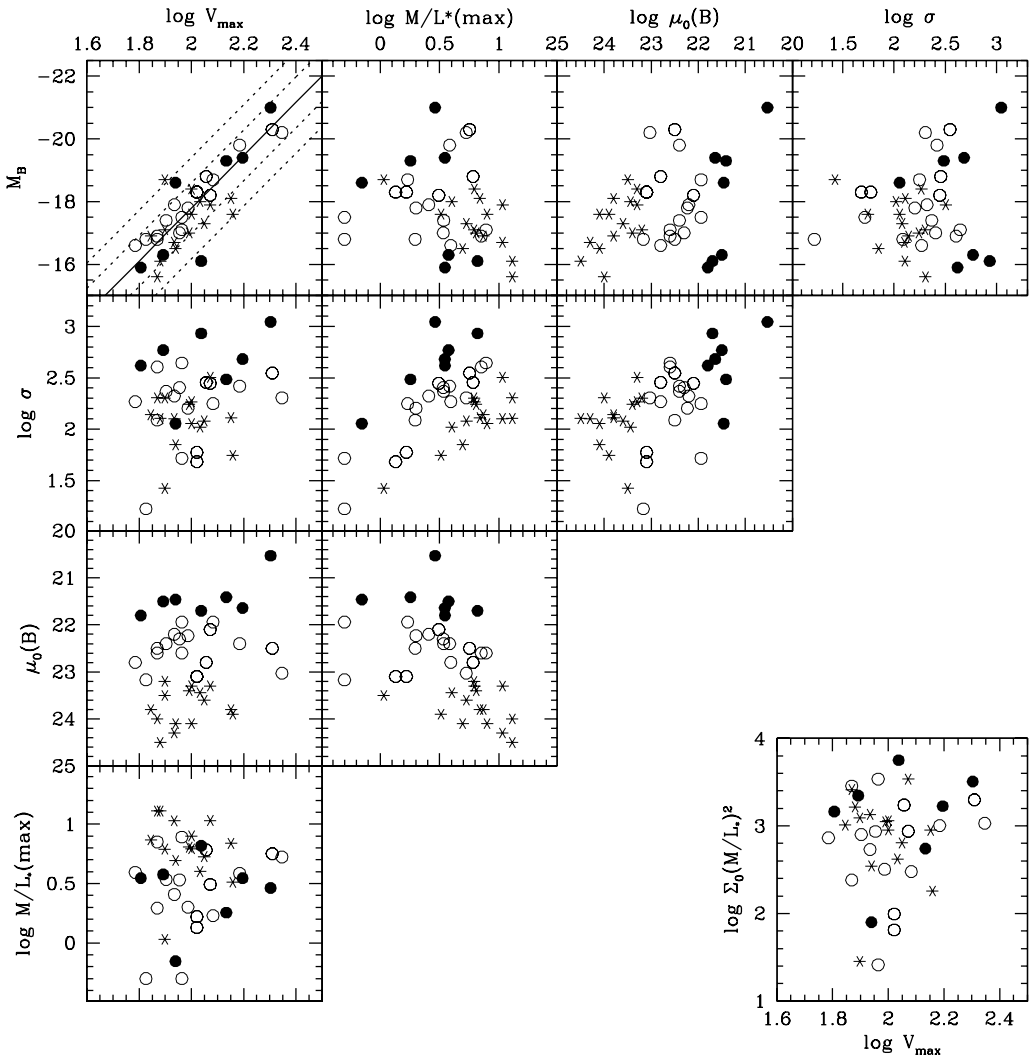

FIG. 14.— Correlations between maximum disk surface density $\sigma[M_\odot\ \mathrm{pc}^{-2}]$, surface brightness $\mu_0[B\text{-mag arcsec}^{-2}]$, maximum disk $\Upsilon_\star(\mathrm{B})$ $[M_\odot/L_{\odot,B}]$, maximum observed rotation velocity $V_{\max}$ [km s^{-1}] and luminosity M_B [mag]. Included are again the bulge-less bright HSB galaxies from Broeils (1992) and the high-quality curves of bright dwarfs from Swaters (1999), as described in the previous figure caption. Black circles: $\mu_0(B) < 21.9$ mag arcsec^{-2}; open circles: $21.9 \leq \mu_0(B) \leq 23.2$; stars: $\mu_0(B) > 23.2$ mag arcsec^{-2}. The inset panel in the lower-right corner shows the product $\Sigma_0(\Upsilon_*)^2$, where Σ_0 is the central surface brightness expressed in $L_\odot$ pc^{-2}. This product should be constant with small scatter for a maximum disk interpretation of the TF relation. The TF relation is shown in the top-left corner. It has a slope of -8.4. The dotted lines represent the 1σ and 2σ scatter where $\sigma = 0.81$ mag. This scatter is reduced to 0.51 mag when the 4 most outlying points are omitted (all galaxies with low inclinations).

TABLE 1
SAMPLE I: GALAXIES WITH PHOTOMETRY

Name	D	$\mu_0(B)$	h	$M_{\rm abs}(B)$	$R_{\rm max}$	$V_{\rm max}$	$V_{\rm hel}$	i
	(Mpc)	(mag/□")	(kpc)	(mag)	(kpc)	(km s^{-1})	(km s^{-1})	(°)
(1)	(2)	(3)	(4)	(5)	(6)	(7)	(8)	(9)
F563-1	45	23.6	2.8	-17.3	17.7	112	3502	25
F563-V2	61	22.1	2.1	-18.2	9.2	118	4312	29
F568-1	85	23.8	5.3	-18.1	14.9	142	6524	26
F568-3	77	23.1	4.0	-18.3	16.5	105	5913	40
F568-V1	80	23.3	3.2	-17.9	19.0	118	5768	40
F571-8	48	23.9[a]	5.2	-17.6[a]	15.6	144	3768	90
F574-1	96	23.3[a]	4.3	-18.4[a]	15.4	100	6889	65
F579-V1	85	22.8[a]	5.1	-18.8[a]	17.3	114	6305	26
F583-1	32	24.1	1.6	-16.5	14.6	87	2264	63
F583-4	49	23.8[a]	2.7	-16.9[a]	10.0	70	3617	55
U5750	56	23.5[a]	5.6	-18.7[a]	21.8	79	4177	64
U6614	85	23.4	8.1	-20.3	62	204	6371	36

Note. — (2) Distance computed assuming Hubble flow after correction for galactic rotation and Virgocentric flow. (6) Maximum radius of rotation curve. (7) Maximum velocity in rotation curve. (8) Heliocentric systemic velocity. Photometric and distance data from de Blok & McGaugh (1997). $R_{\rm max}$, $V_{\rm max}$ and $V_{\rm sys}$ derived from new optical curves.

[a]Converted from R-band assuming $B-R=0.9$.

TABLE 2
SAMPLE II: GALAXIES WITHOUT PHOTOMETRY

Name	D	$V_{\rm hel}$	$M_{\rm abs}(B)$	$R_{\rm max}$	$V_{\rm max}$	i
	(Mpc)	(km s^{-1})	(mag)	(kpc)	(km s^{-1})	(°)
(1)	(2)	(3)	(4)	(5)	(6)	(7)
F730-V1	144	10714	···	11.9	145	50
U4115	3.2	343	-12.4	1.0	40	74
U11454	91	6628	-18.6[a]	11.9	152	64
U11557	22	1390	-20.0	6.2	95	36
U11583	5	128	-14.0[a]	1.5	36	83
U11616	73	5244	-20.3[a]	9.6	143	60
U11648	48	3350	-21.0[a]	12.7	145	90
U11748	73	5265	-22.9[a]	21.0	242	78
U11819	60	4261	-20.3[a]	11.7	153	66
E0140040	212	16064	-21.6	29.2	263	35
E0840411	80	6200	-18.1	8.9	61	90
E1200211	15	1314	-15.6	3.5	25	70
E1870510	18	1410	-16.5	3.0	40	58
E2060140	60	4704	-19.2	11.6	118	39
E3020120	69	5311	-19.1	11.0	86	55
E3050090	11	1019	-17.3	4.8	54	53
E4250180	86	6637	-20.5	14.4	145	33
E4880049	22	1800	-16.8	6.0	97	63

Note. — Columns (2) and (3): distance D was calculated from $V_{\rm hel}$ after correcting for galactic rotation and assuming pure Hubble flow with $H_0 = 75$ km s^{-1} Mpc^{-1}. Column (4): Absolute magnitude computed using apparent magnitudes from ESO-LV and RC3, and are corrected for foreground Galactic extinction.

[a]The apparent magnitude is Zwicky magnitude 17, and therefore very uncertain.

Table 3
Modeled Rotation Curves

Galaxy	R (arcsec)	R (kpc)	V_{gas} [a,b] (km/s)	V_{disk} [a,c] (km/s)	V_{bulge} [a,c] (km/s)	V_{obs} (km/s)	σ_V (km/s)
F583-1							
	0.3	0.1	-0.1	0.4	0	1.1	11.1
	2.8	0.4	-0.9	4.0	0	10.0	7.0
	5.0	0.7	-1.5	6.7	0	17.4	9.6
	6.9	1.0	-2.2	8.5	0	23.5	11.2
	9.0	1.4	-2.8	10.1	0	31.0	5.2

[a]Only given when known (Sample I). Set to zero if unknown.

[b]Assumes $M_{gas} = 1.4 M_{HI}$.

[c]For $M/L = 1.0$ in the R-band.

Note. — The complete version of this table is in the electronic edition of the Journal. The printed edition contains only a sample. These data are also available in electronic format from http://www.atnf.csiro.au/∼edeblok/data and http://www.astro.umd.edu/∼ssm/data.

Table 4
Comparison of fitting parameters

			NFW halo, minimum disk				
Galaxy	Obs	Curve	c	Δc	V_{200}	ΔV_{200}	χ^2_{red}
F563-V2	SMT	SMT	16.2	3.4	84.5	10.4	2.516
F563-V2	SMT	dBMR	7.5	3.7	153.1	70.5	1.391
F563-V2	SMT	data	5.9	2.2	192.3	76.4	3.42
F568-1	SMT	SMT	13.4	1.1	112.1	6.3	0.265
F568-1	SMT	dBMR	6.4	2.5	194.6	71.9	0.804
F568-1	SMT	data	8.3	1.1	154.5	18.5	3.49
F568-3	SMT	SMT	5.1	2.9	160.3	88.0	2.147
F568-3	SMT	dBMR	*1.17*	···	*591.0*	···	3.551
F568-3	SMT	data	1.71	0.5	400.4	94.8	13.9
F568-3	Paper I	dBMR	3.2	3.7	214.6	233.9	2.239
F568-3	Paper I	data[a]	4.6	0.5	168.4	17.7	8.01
F568-V1	SMT	SMT	14.2	0.7	91.5	2.3	0.239
F568-V1	SMT	dBMR	14.6	1.2	92.1	4.9	0.197
F568-V1	SMT	data	15.8	1.1	85.7	3.8	12.7
F574-1	SMT	SMT	9.4	0.7	91.2	4.3	0.421
F574-1	SMT	dBMR	8.3	1.3	98.3	10.4	1.595
F574-1	SMT	data	8.2	0.4	99.3	3.4	3.84

Note. — Italics indicate estimates, not actual fits. V_{200} is in km s^{-1}. The column labeled "Obs" gives the source of the raw data. The column labeled "Curve" gives the source for the derived rotation curve: "SMT" indicates smooth rotation curve from SMT; "dBMR" indicates smooth rotation curve from this paper; "data" indicates a fit to the raw data.

[a]Uncertain, depends on initial estimates of fit.

TABLE 5
FITTING PARAMETERS NFW HALO, SAMPLE I

	minimum disk						minimum disk + gas					
Galaxy	c	Δc	V_{200}	ΔV	χ^2_{red}	p	c	Δc	V_{200}	ΔV	χ^2_{red}	p
F563-1	10.7	1.2	93.1	4.3	0.092	0.999	11.3	1.3	87.5	3.9	0.089	0.999
F568-3	3.2	3.7	214.6	233.9	2.239	0.017	4.2	3.3	161.3	118.9	2.386	0.011
F571-8	7.8	1.1	163.8	20.2	1.501	0.123	7.8	1.1	163.3	20.1	1.477	0.132
F579-V1	20.9	1.5	78.4	2.6	0.211	0.998	22.1	1.6	75.1	2.5	0.217	0.998
F583-1	5.1	1.0	106.6	17.0	0.740	0.746	6.2	1.1	86.6	12.4	0.827	0.648
F583-4	5.7	1.4	89.5	19.0	0.322	0.944	6.1	1.4	82.2	15.5	0.321	0.945
U5750	2.6	1.5	123.1	58.8	1.243	0.262	2.9	1.6	105.8	47.7	1.203	0.288
U6614	10.3	2.0	169.8	17.7	4.626	0.000	11.0	2.2	163.9	17.1	4.712	0.000
SMT data, our analysis												
F563-V2	7.5	3.7	153.1	70.5	1.391	0.195	8.3	3.8	133.1	54.1	1.484	0.157
F568-1	6.4	2.4	194.6	71.9	0.804	0.625	7.5	2.4	160.1	46.7	0.869	0.562
F568-3	*1.2*	···	*591.1*	···	3.551	0.000	*1.2*	···	*552.6*	···	3.573	0.000
F568-V1	14.6	1.2	92.0	4.9	0.197	0.999	15.7	1.5	87.2	5.0	0.242	0.997
F574-1	8.3	1.3	98.3	10.4	1.595	0.085	9.0	1.5	91.1	9.4	1.806	0.041

	constant $\Upsilon_\star(R) = 1.4$						maximum disk						
Galaxy	c	Δc	V_{200}	ΔV	χ^2_{red}	p	c	Δc	V_{200}	ΔV	χ^2_{red}	p	Υ^R_*
F563-1	9.9	1.2	88.8	4.6	0.089	0.999	4.0	1.2	110.0	20.1	0.098	0.999	6.9
F568-3	2.3	4.9	218.6	410.9	2.127	0.024	0.4	19.5	595.0	∞	2.015	0.024	2.2
F571-8	1.6	5.7	591.4	···	3.776	0.012	*1.0*	···	*500.0*	···	7.060	0.000	4.2
F579-V1	23.2	1.9	67.9	2.4	0.215	0.998	43.4	14.6	31.6	3.9	0.671	0.781	7.9
F583-1	5.4	1.1	90.6	14.7	0.767	0.716	2.2	1.5	145.5	78.7	0.680	0.804	6.5
F583-4	5.9	1.4	76.0	14.5	0.271	0.965	11.4	6.1	12.9	3.3	0.196	0.986	9.6
U5750	1.9	1.7	116.9	80.4	1.105	0.354	1.9	1.7	116.9	80.4	1.105	0.354	1.4
U6614	1.7	1.8	303.0	206.5	4.005	0.001	*0.4*	···	*145.6*	···	7.828	0.737	7.7
SMT data, our analysis													
F563-V2	6.5	3.8	136.0	73.3	1.047	0.397	*1.0*	···	*350.0*	···	0.449	0.878	4.1
F568-1	6.7	2.5	163.8	56.1	0.803	0.626	*0.6*	···	*669.2*	···	0.636	0.898	9.0
F568-3	*1.0*	···	*519.4*	···	3.595	0.000	*1.0*	···	*467.8*	···	3.624	0.000	1.8
F568-V1	14.6	1.4	88.8	5.3	0.228	0.998	3.3	1.5	125.8	45.7	0.222	0.998	14.0
F574-1	8.2	1.4	87.1	9.5	1.391	0.162	1.5	1.6	69.7	43.9	0.204	0.998	8.1

Note. — Italics indicate estimates, not actual fits. V_{200} is in km s^{-1}.

TABLE 6
FITTING PARAMETERS NFW HALO, SAMPLE II

	minimum disk					
Galaxy	c	Δc	V_{200}	ΔV	χ^2_{red}	p
F730-V1	11.8	1.9	131.4	16.2	0.995	0.426
U4115	*5.0*	···	*133.4*	···	0.777	0.591
U11454	10.4	2.0	152.6	23.3	3.334	0.000
U11557	*1.0*	···	*425.1*	···	1.367	0.093
U11583	*5.0*	···	*93.3*	···	0.676	0.641
U11616	12.7	1.8	124.4	14.3	1.254	0.244
U11648	8.0	0.7	146.2	10.9	0.964	0.498
U11748	52.5	4.5	125.2	3.8	3.325	0.000
U11819	6.4	1.9	252.9	77.6	1.348	0.177
E0140040	16.8	0.8	203.3	5.8	0.152	0.989
E0840411	*1.0*	···	*181.0*	···	1.608	0.077
E1200211	6.4	2.1	27.5	6.9	0.246	0.996
E1870510	3.8	1.5	93.6	38.6	0.059	1.000
E2060140	15.2	1.3	92.7	4.4	0.425	0.962
E3020120	6.6	1.5	98.5	18.4	0.333	0.965
E3050090	*1.0*	···	323.6	···	0.208	0.999
E4250180	3.1	0.9	301.6	77.8	0.014	1.000
E488-049	4.9	1.9	209.6	90.1	0.170	0.999

Note. — Italics indicate estimates, not actual fits. V_{200} is in km s^{-1}.

TABLE 7
FITTING PARAMETERS ISO HALO, SAMPLE I

	minimum disk						minimum disk + gas					
Galaxy	R_C	ΔR	ρ_0	$\Delta\rho$	χ^2_{red}	p	Rc	ΔR	ρ_0	$\Delta\rho$	χ^2_{red}	p
F563-1	1.72	0.23	91.9	21.6	0.085	1.000	1.55	0.22	102.0	25.2	0.078	1.000
F568-3	2.92	0.36	36.6	5.4	0.522	0.860	2.71	0.39	38.3	6.8	0.676	0.731
F571-8	2.12	0.19	106.9	14.0	1.525	0.114	2.12	0.19	106.3	14.0	1.512	0.118
F579-V1	0.67	0.02	574.8	37.3	0.026	1.000	0.63	0.03	630.8	50.2	0.037	1.000
F583-1	2.44	0.06	33.0	1.1	0.037	1.000	2.08	0.11	37.7	2.5	0.117	1.000
F583-4	1.10	0.13	85.5	15.8	0.329	0.941	1.06	0.11	88.2	15.1	0.267	0.967
U5750	4.25	0.39	10.6	1.0	0.154	0.998	3.96	0.49	10.4	1.3	0.214	0.993
U6614	1.86	0.49	218.4	102.5	1.942	0.021	1.73	0.44	244.7	111.6	1.777	0.040
SMT data, our analysis												
F563-V2	1.69	0.17	131.2	19.4	0.283	0.972	1.58	0.20	135.3	24.7	0.393	0.925
F568-1	2.22	0.10	97.2	6.2	0.066	1.000	2.03	0.12	104.6	8.9	0.106	1.000
F568-3	3.93	0.75	30.2	5.6	1.256	0.245	3.75	0.78	30.8	6.3	1.383	0.173
F568-V1	1.45	0.11	153.0	18.2	0.110	1.000	1.33	0.14	170.0	27.8	0.172	1.000
F574-1	1.83	0.06	71.5	3.7	0.100	1.000	1.70	0.09	76.9	6.3	0.232	0.997

	constant $\Upsilon_\star(R) = 1.4$						maximum disk						
Galaxy	R_C	ΔR	ρ_0	$\Delta\rho$	χ^2_{red}	p	R_C	ΔR	ρ_0	$\Delta\rho$	χ^2_{red}	p	$\Upsilon^R_\star$
F563-1	1.72	0.26	79.0	21.3	0.083	1.000	4.09	1.01	13.2	4.9	0.124	0.998	6.9
F568-3	3.07	0.63	25.7	6.3	0.793	0.623	3.36	0.88	19.7	5.9	0.89	0.536	2.2
F571-8	4.19	0.28	34.4	2.7	0.405	0.954	9.97	3.43	9.8	2.3	2.639	0.002	4.2
F579-V1	0.55	0.04	694.4	84.0	0.06	1.000	0.17	0.16	1970	3234	1.032	0.415	7.9
F583-1	2.26	0.11	31.5	2.0	0.103	1.000	3.41	0.24	14.3	1.2	0.121	1.000	6.5
F583-4	1.02	0.12	80.6	15.2	0.249	0.972	0.23	0.15	103.4	114.1	0.188	0.988	9.6
U5750	4.67	0.74	7.1	1.1	0.262	0.984	4.67	0.74	7.1	1.1	0.262	0.984	1.4
U6614	12.18	2.87	6.3	1.9	1.938	0.022	112.0	506.7	0.4	0.4	4.762	0.000	7.4
SMT data, our analysis													
F563-V2	1.70	0.24	96.6	19.8	0.298	0.967	2.32	0.63	30.8	11.5	0.191	0.992	4.1
F568-1	2.11	0.15	90.7	9.0	0.120	1.000	3.08	0.73	27.6	8.5	0.270	0.988	9.0
F568-3	4.35	1.31	21.5	6.0	1.709	0.065	4.54	1.52	19.4	5.9	1.815	0.046	1.8
F568-V1	1.41	0.15	146.1	23.0	0.153	1.000	3.80	0.58	14.8	2.6	0.120	1.000	14.0
F574-1	1.74	0.09	63.1	5.4	0.182	0.999	3.30	0.83	4.6	1.6	0.108	1.000	8.1

Note. — R_C is in kpc. ρ_0 is expressed in units of 10^{-3} $M_\odot$ pc^{-3}.

Table 8
Fitting parameters ISO halo, Sample II

	minimum disk					
Galaxy	R_C	ΔR	ρ_0	$\Delta\rho$	χ^2_{red}	p
F730-V1	1.46	0.06	215.8	14.2	0.097	0.997
U4115	0.94	0.03	148.2	2.4	0.004	1.000
U11454	1.95	0.10	146.9	11.8	0.423	0.927
U11557	5.48	0.55	15.2	0.9	0.052	1.000
U11583	0.63	0.08	117.8	16.5	0.103	0.999
U11616	1.45	0.05	208.9	11.6	0.140	1.000
U11648	1.95	0.25	104.9	20.7	3.792	0.000
U11748	0.36	0.15	8540	6661	5.402	0.000
U11819	2.93	0.14	88.2	5.2	0.303	0.991
E0140040	2.55	0.18	249.5	27.0	0.176	0.982
E0840411	6.41	0.56	5.2	0.3	0.067	0.999
E1200211	0.57	0.08	45.5	9.2	0.082	1.000
E1870510	0.97	0.05	53.5	3.2	0.028	1.000
E2060140	1.17	0.05	231.1	16.9	0.106	1.000
E3020120	1.90	0.09	53.6	3.4	0.035	1.000
E3050090	2.09	0.14	27.3	1.8	0.048	1.000
E4250180	4.41	0.75	30.0	6.6	0.088	0.997
E488-049	1.63	0.04	101.1	3.1	0.016	1.000

Note. — R_C is in kpc. ρ_0 is expressed in units of 10^{-3} $M_\odot$ pc^{-3}.

Table 9
Comparison probabilities NFW vs. ISO Sample I

	Number of galaxies (out of 13)			
	ISO halo		NFW halo	
$\Upsilon_\star$	$p > 0.95$	$p < 0.05$	$p > 0.95$	$p < 0.05$
minimum	8	1	4	3
min+gas	8	1	4	4
constant	10	1	4	4
maximum	8	3	6	3

Note. — p is the probability that the model is compatible with the data.

Table 10
Morphology and probability NFW halos

Galaxy	prob.[a]	core[b]	bar[b]	morphology
F563-1	+	–	+	mag. irr.
F563-V2	0	–	+	mag. bar
F568-1	0	+	–	spiral
F568-3	–	–	+	spiral with mag. bar
F568-V1	+	+	–	spiral
F571-8	0	+	?	edge-on
F574-1	–	+	–	disk
F579-V1	+	+	–	core, flocc. arms
F583-1	0	+	–	mag. irr.
F583-4	+	+?	+?	fuzzy
F730-V1	0	+	–	spiral
U4115	0	+?	–	fuzzy
U5750	0	–	+	mag. bar
U6614	–	+	–	faint, with bulge
U11454	–	+	–	fuzzy spiral, small core
U11557	0	+	–	fuzzy spiral, small core
U11583	0	–	+	faint mag. bar
U11616	0	+	–	fuzzy, irr
U11648	0	–	+	irr
U11748	–	+	+?	irr, bright core/bar?
U11819	0	+	–	fuzzy
E0140040	+	+	–	spiral
E0840411	–	–	?	edge-on
E1200211	+	–	+	fuzzy mag. bar
E1870510	+	–	+	irr. spiral, flocc.
E2060140	+	+	–	spiral
E3020120	+	+	+?	spiral, hint of bar?
E3050090	+	+	+	barred spiral
E4250180	+	+	–	spiral
E488-049	+	–	+	inclined mag. bar

[a] "+" indicates good fit $p \geq 0.95$; "0" indicates average fit $0.05 < p < 0.95$; "–" indicates bad fit $p < 0.05$.

[b] "+" indicates component clearly present; "–" indicates component not obviously present.

Table 11
Morphology and probability NFW halos

quality	bar	core	both
good ($p > 0.95$)	4	7	3
bad ($p < 0.05$)	2	4	0
unclear ($0.05 < p < 0.95$)	4	7	1

Note. — Value indicates number of minimum disk fits of that quality in presence of component mentioned.